Geophysical Journal International

Geophys. J. Int. (2014) **199,** 1878–1899 doi: 10.1093/gji/ggu341
GJI Geodynamics and tectonics

A new GPS velocity field for the Pacific Plate – Part 1: constraints on plate motion, intraplate deformation, and the viscosity of Pacific basin asthenosphere

C. DeMets,[1] Bertha Márquez-Azúa[2] and Enrique Cabral-Cano[3]

[1]*Department of Geoscience, University of Wisconsin-Madison, Madison, WI* 53706, *USA. E-mail: chuck@geology.wisc.edu*
[2]*Centro Universitario de Ciencias Sociales y Humanidades, Universidad de Guadalajara, Guadalajara, Jalisco* 44660, *Mexico*
[3]*Departmento de Geomagnetismo y Exploración, Instituo de Geofisica, Universidad Nacional Autónoma de México, Ciudad Universitaria,* 04510 *México, D.F., Mexico*

Accepted 2014 September 4. Received 2014 September 3; in original form 2014 May 6

SUMMARY

We combine new, well-determined GPS velocities from Clarion, Guadalupe and Socorro islands on young seafloor in the eastern Pacific basin with newly estimated velocities for 26 GPS sites from older seafloor in the central, western and southern parts of the Pacific Plate to test for deformation within the interior of the Pacific Plate and estimate the viscosity of the asthenosphere below the plate. Relative to a Pacific Plate reference frame defined from the velocities of the 26 GPS sites in other areas of the Pacific Plate, GPS sites on Clarion and Guadalupe islands in the eastern Pacific move 1.2 ± 0.6 mm yr^{-1} (1σ) towards S09°W $\pm$ 38° and 1.9 ± 0.3 mm yr^{-1} towards S19°E $\pm$ 10°, respectively. The two velocities, which are consistent within their 95 per cent uncertainties, both differ significantly from Pacific Plate motion. Transient volcanic deformation related to a 1993–1996 eruption of the Socorro Island shield volcano renders our GPS velocity from that island unreliable for the tectonic analysis although its motion is also southward like those of Clarion and Guadalupe islands. We test but reject the possibilities that drift of Earth's origin in ITRF2008 or unmodelled elastic offsets due to large-magnitude earthquakes around the Pacific rim since 1993 can be invoked to explain the apparent slow southward motions of Clarion and Guadalupe islands. Similarly, corrections to the Pacific Plate GPS velocity field for possible viscoelastic deformation triggered by large-magnitude earthquakes since 1950 also fail to explain the southward motions of the two islands. Viscoelastic models with prescribed asthenospheric viscosities lower than 1×10^{19} Pa s instead introduce statistically significant inconsistencies into the Pacific Plate velocity field, suggesting that the viscosity of the asthenosphere below the plate is higher than 1×10^{19} Pa s. Elastic deformation from locked Pacific–North America Plate boundary faults is also too small to explain the southward motions of the two islands. Horizontal thermal contraction of the plate interior may explain the motion observed at Clarion and Guadalupe islands, as might long-term tectonic deformation of the plate interior.

Key words: Plate motions; Rheology: mantle; Pacific Ocean.

1 INTRODUCTION

As the largest of the tectonic plates, the Pacific Plate has long been recognized as a superb setting for geodetic studies of a broad range of geophysical topics, including plate motions, the limits of the rigid plate hypothesis, natural hazards and thermal cooling of the lithosphere. Geodetic efforts to measure present-day Pacific–North America Plate motion and estimate deformation within the Pacific Plate began with satellite laser ranging (SLR) measurements in 1978 on the Pacific islands of Mauai and Huahine (Smith *et al.* 1990) and were augmented in 1984 with very-long-baseline interferometric (VLBI) measurements on the islands of Kauai and Kwajalein (Ryan *et al.* 1993). Analyses of these data detected no significant deformation of the plate interior within their several millimetres per year uncertainties (Smith *et al.* 1990; Ryan *et al.* 1993; Argus & Gordon 1996).

By the mid 1990s, Global Positioning System (GPS) measurements had largely supplanted SLR and VLBI measurements on the Pacific Plate. In support of the earlier results from SLR and VLBI data, studies of GPS observations that span longer time periods and

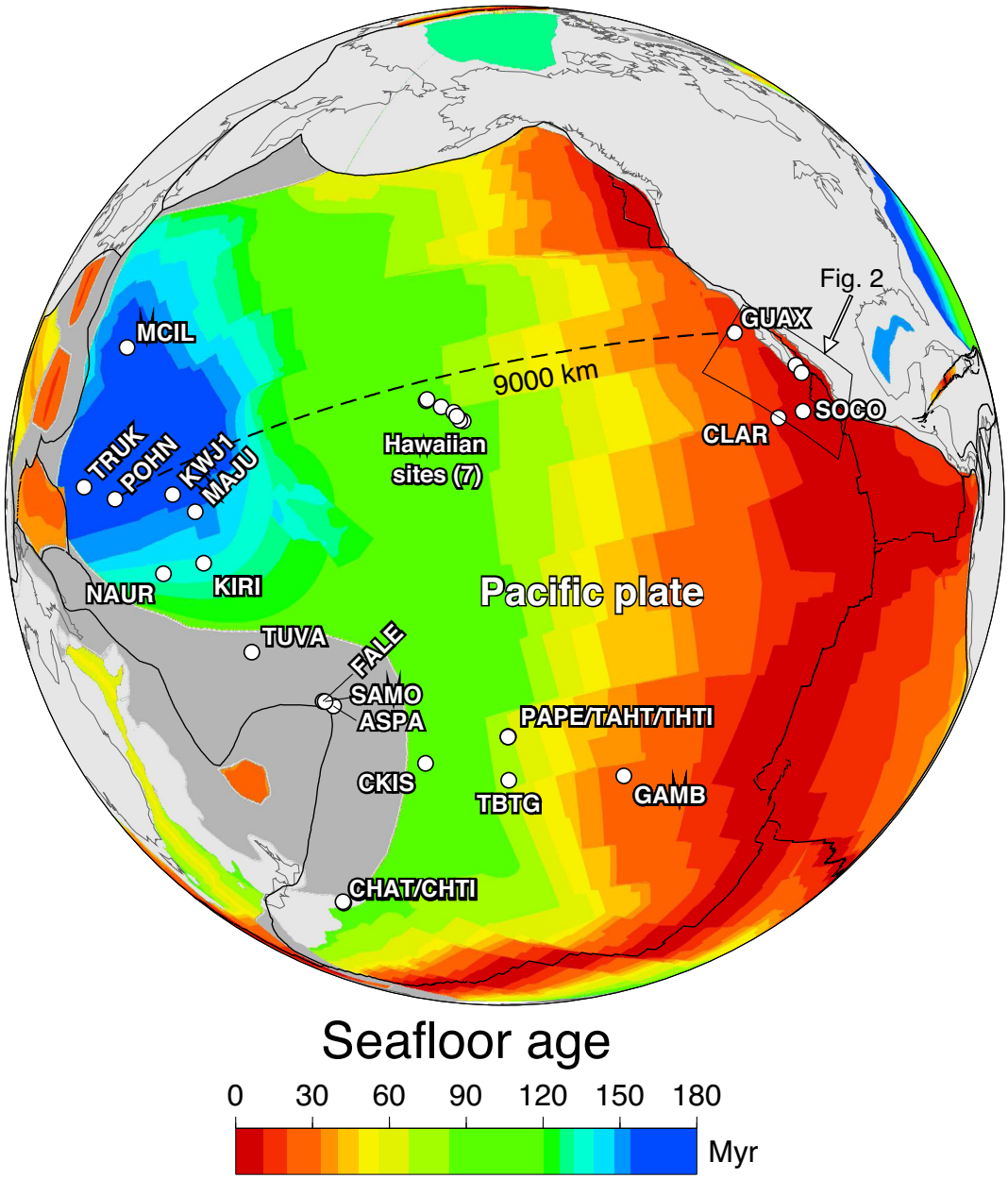

Figure 1. Locations (open circles) and names of GPS sites used to study motion and deformation of the Pacific Plate. Seafloor ages are from Muller *et al.* (1997).

larger areas of the plate interior than did SLR and VLBI data also found no evidence for significant internal deformation of the plate. For example, results reported by Larson *et al.* (1997), DeMets & Dixon (1999), Beavan *et al.* (2002), Tregoning (2002), Gonzalez-Garcia *et al.* (2003), Marquez-Azua *et al.* (2004), Plattner *et al.* (2007) and Argus *et al.* (2010) imply strain rates within the older areas of the Pacific Plate of only 10^{-11} to 10^{-10} yr^{-1}, consistent with the low level of seismicity in the plate interior during much of the past century (Wysession *et al.* 1991).

In this study, we present a new Pacific Plate GPS velocity field that includes for the first time well-determined velocities from each of Clarion, Guadalupe and Socorro islands (Fig. 1), the only three locations on the eastern 40 per cent of the Pacific Plate interior where GPS measurements are logistically feasible. The new velocity field enables the strongest geodetic test to date for active deformation across the entire ≈10 000 km east-to-west expanse of the Pacific Plate (Fig. 1), spanning seafloor ages from ≈190 to 3 Ma. We examine the consistency of the new velocity field with several hypotheses for the sources of deformation within the plate, including viscoelastic deformation from historic earthquakes (Pollitz *et al.* 1998) and horizontal thermal contraction between young and old seafloor (Kumar & Gordon 2009). We also use the new velocity field to test for possible drift of Earth's origin in the ITRF2008 geodetic reference frame and to test whether offsets from large earthquakes may bias the velocities estimated at some GPS sites (Tregoning *et al.* 2013). In a companion paper (DeMets *et al.* 2014), we use the results presented herein to revisit the important topic of how much deformation occurs on slowly slipping, but seismically hazardous faults in western California such as the Rinconada, Hosgri, San Gregorio and San Simeon faults.

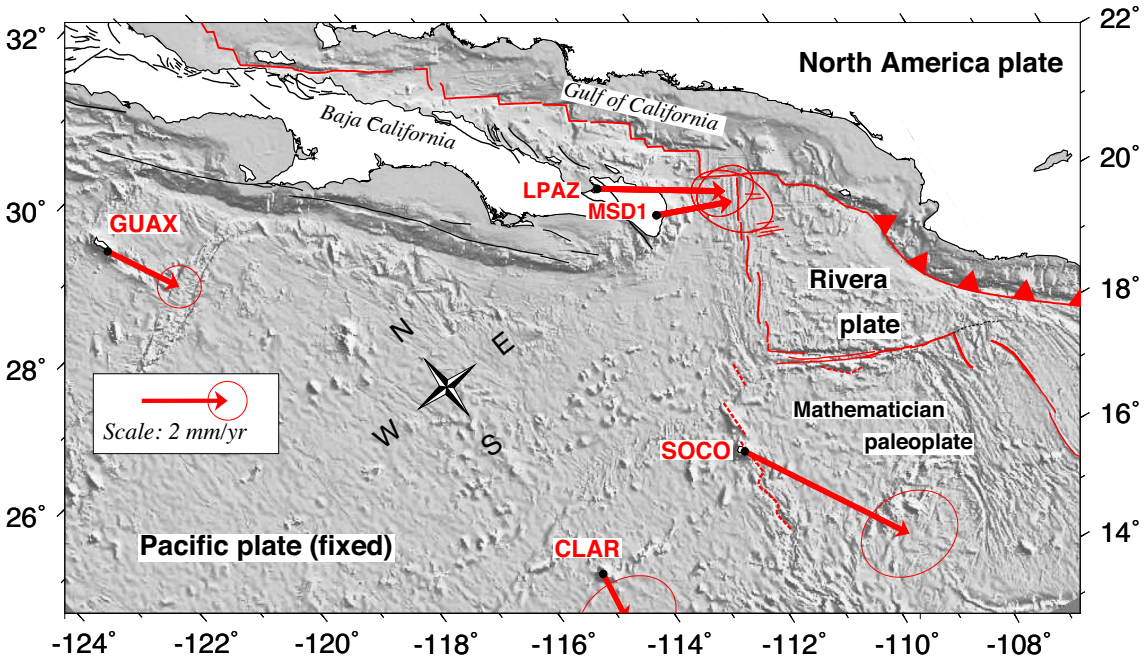

Figure 2. Velocities of GPS sites on Clarion (CLAR), Guadalupe (GUAX) and Socorro (SOCO) islands and continuous GPS sites LPAZ and MSD1 corrected for the motion of the Pacific Plate relative to ITRF2008 (Table 2). Velocity ellipses are 1σ, 2-D. Map projection is oblique Mercator.

2 GPS DATA

Measurements from 29 GPS sites on the Pacific Plate are used for the analysis. Important new data include campaign measurements we collected in 2013 from GPS sites CLAR on Clarion Island and SOCO on Socorro Islands in the eastern Pacific (Fig. 2), and continuous and quasi-continuous measurements from sites in the Austral, Gambier and Society Islands in Polynesia (labelled TBTG, GAMB and PAPE in Fig. 1), and Chatham Island (CHTI also in Fig. 1). The former data extend the GPS time-series on Clarion and Socorro islands by 13 yr relative to the still-immature 3-yr-long time-series that were previously reported by Marquez-Azua *et al.* (2004). Data from the latter four sites provide much needed redundancy in the central and southern areas of the Pacific Plate and have not to our knowledge been used in a study such as this.

2.1 Campaign data

Clarion Island is located ≈1000 km west of Mexico on 13.5-Myr-old Pacific Plate seafloor (Klitgord & Mammerickx 1982). Socorro Island, an active shield volcano on the extinct Mathematician rise (Fig. 2), is located ≈650 km west of Mexico on ≈3.2-Myr-old seafloor (Mammerickx *et al.* 1988). Our GPS monuments on both islands consist of 9-inch stainless steel pins that are epoxied into basalt, the former in a basalt flow and the latter in a large, buried basalt boulder. Guadalupe Island, the other island in the eastern Pacific from which we use GPS data, is located on the extinct Guadalupe rift, which ceased spreading at ≈12.5 Ma (Lonsdale 1991). These are the only three islands on the eastern 40 per cent of the Pacific Plate that are accessible for GPS measurements and, moreover, are the only Pacific Plate islands that are located on seafloor younger than 20 Myr.

The Clarion Island GPS site was occupied for 14 d in 1997, 5 d in 1999, 7 d in 2000 and 11 d in 2013, spanning 15.6 yr. The Socorro island site was occupied for 16 d in 1997, 12 d during two occupations in 1999, 7 d in 2000 and 12 d in 2013, also spanning 15.6 yr. Both sites were occupied with Trimble GPS receivers and choke-ring or Zephyr geodetic antennas.

The velocity for station GUAX on Guadalupe Island is based on two occupations of campaign site GAIR (in 1993 and 1999) and 4.2 yr of nearly continuous measurements at site GUAX from 2001 to 2005. Following Plattner *et al.* (2007), we linked the motions of GAIR and GUAX using a precise tie that was estimated from three days of overlapping observations at the two sites (Table 1 and R. Malservisi personal communication, 2013). We retain the station name GUAX for this hybrid time-series, but note that Plattner *et al.* (2007) named this hybrid site GUAZ. Gonzalez-Garcia *et al.* (2003) describe velocities for two other campaign sites on Guadalupe Island (RGMU and GUAD); however, the data for those sites were unavailable for this study.

2.2 Continuous data

Continuous data from the other 26 Pacific Plate stations used for our analysis were procured from the Scripps Orbit and Permanent Array Center (SOPAC), the National Geodetic Survey CORS archive, the U.S. Defense Mapping Agency, Geoscience Australia, and SONEL, an archiving facility for GPS sites that are colocated with tide gauges (www.sonel.org). The observations span 10.1–17.3 yr for 21 of the 26 sites and 4.8–6.8 yr for the remaining sites (Table 1).

3 GPS DATA ANALYSIS, COORDINATE TIME-SERIES AND VELOCITIES

3.1 Analysis methods

All of the GPS data described above were processed with release 6.2 of the GIPSY software suite from the Jet Propulsion Laboratory (JPL). Daily GPS station coordinates were first estimated in a no-fiducial reference frame using a precise point-positioning strategy (Zumberge *et al.* 1997). The analysis

Table 1. Pacific Plate GPS site motions in ITRF2008.

Site code	Lat. (°N)	Long. (°E)	V_e (mm yr^{-1})	V_n (mm yr^{-1})	Corr. coeff.	Time (yr)
ASPA	−14.326	189.278	−63.5 ± 0.3	34.1 ± 0.3	−0.7166	12.452
CHAT	−43.956	183.434	−40.5 ± 0.3	33.0 ± 0.3	0.1171	16.421
CHTI	−43.736	183.383	−41.2 ± 0.5	32.1 ± 0.5	0.0692	6.090
CKIS	−21.201	200.199	−62.7 ± 0.4	35.3 ± 0.3	−0.0681	12.392
CLAR	18.341	245.265	−56.3 ± 0.8	23.7 ± 0.6	0.0000	15.567
FALE	−13.832	188.000	−63.7 ± 0.3	33.4 ± 0.3	0.4346	16.123
GMBI	−23.130	225.035	−67.5 ± 0.4	32.0 ± 0.4	0.0951	10.488
GUAX[1]	28.884	241.710	−47.3 ± 0.3	24.6 ± 0.3	0.0106	11.959
HILO	19.719	204.947	−62.4 ± 0.3	35.6 ± 0.3	0.1881	12.896
HNLC	21.303	202.135	−62.6 ± 0.3	34.6 ± 0.3	0.3373	16.616
KIRI	1.355	172.923	−67.9 ± 0.3	31.3 ± 0.3	0.0548	11.501
KOK1	21.984	200.242	−62.1 ± 0.4	35.2 ± 0.3	0.1502	11.748
KOKB	22.126	200.335	−62.1 ± 0.3	34.7 ± 0.3	0.1232	14.082
KWJ1	8.722	167.730	−68.8 ± 0.6	29.5 ± 0.5	0.1503	6.348
LPAZ	24.139	249.681	−48.3 ± 0.5	21.1 ± 0.3	0.0061	18.663
MAJU	7.119	171.365	−69.0 ± 0.5	30.5 ± 0.4	0.0207	6.696
MAUI	20.707	203.743	−61.9 ± 0.3	34.7 ± 0.3	0.1247	15.082
MCIL	24.290	153.979	−71.7 ± 0.3	23.8 ± 0.3	−0.0563	11.148
MKEA	19.801	204.544	−62.4 ± 0.3	34.9 ± 0.3	0.0918	17.331
MSD1	23.160	250.282	−49.8 ± 0.5	21.9 ± 0.6	−0.3468	5.776
NAUR	−0.552	166.926	−67.0 ± 0.3	29.6 ± 0.4	−0.0442	10.592
PAPE	−17.533	210.427	−66.6 ± 0.5	34.2 ± 0.4	0.0717	10.140
POHN	6.960	158.210	−70.2 ± 0.3	26.1 ± 0.4	0.0774	10.748
SAMO	−13.849	188.262	−63.8 ± 0.3	33.4 ± 0.3	0.6439	12.586
SOCO	18.728	249.055	−53.2 ± 0.8	19.5 ± 0.6	0.0000	15.570
TAHT	−17.577	210.394	−65.8 ± 0.4	34.3 ± 0.3	0.0879	13.386
TBTG	−23.342	210.524	−64.5 ± 0.7	33.7 ± 0.6	−0.0323	4.430
THTI	−17.577	210.394	−65.8 ± 0.3	34.5 ± 0.3	0.0746	15.192
TRUK	7.447	151.887	−69.6 ± 0.5	23.8 ± 0.5	0.1142	6.819
TUVA	−8.525	179.197	−63.8 ± 0.3	32.5 ± 0.3	0.1451	12.175
UPO1	20.246	204.116	−61.5 ± 0.7	34.9 ± 0.6	−0.1086	11.929

Notes: Uncertainties in the north and east velocity components V_n and V_e are 1σ. Column 6 gives the correlation coefficient between the north and east velocity variances. Time specifies the interval spanned by the GPS data. Site motions are given relative to ITRF2008. 1 - Time-series for GUAX consists of 3-d and 5-d occupations of campaign site GAIR in 1993 and 1999, respectively, and continuous observations at GUAX from 2001 to 2005. The GAIR and GUAX time-series are linked via a site tie determined from 3 d of simultaneous occupation of the two sites, as follows: $X = -5111.162 \pm 0.003$ m, $Y = -5371.582 \pm 0.007$ m and $Z = -14004.189 \pm 0.003$ m (R. Malservisi personal communication, 2013).

incorporated constraints on *a priori* tropospheric hydrostatic and wet delays from Vienna Mapping Function (VMF1) parameters (http://ggosatm.hg.tuwien.ac.at), elevation- and azimuthally dependent GPS and satellite antenna phase center corrections from IGS08 ANTEX files (available via ftp from sideshow.jpl.nasa.gov), FES2004 corrections for ocean tidal loading (http://holt.oso.chalmers.se) and resolution of phase ambiguities via GIPSY's single-station ambiguity resolution feature.

Daily seven-parameter Helmert transformations from JPL were used to transform all daily no-fiducial GPS station positions to IGS08, a GPS-based terrestrial reference frame for which geodetic station velocities map identically into ITRF08 (www.geodesy.noaa.gov/CORS/coords.shtml). For reader convenience, we refer hereafter to the more widely used ITRF08 (Altamimi *et al.* 2011) when we describe the relevant geodetic reference frame. Day-to-day variations in the Pacific Plate station coordinates average 2.2 and 2.4 mm (1σ) in the northing and easting components, respectively.

Best-fitting site velocities (Table 1) and offsets caused by earthquakes or other factors such as GPS hardware changes (Table S1) were estimated via a weighted linear regression of the station position time series. The 2009 September 29 $M_w = 8.0$ Tonga trench earthquakes (Beavan *et al.* 2010; Lay *et al.* 2010) triggered strong transient deformation at GPS stations ASPA, FALE, SAMO and TUVA, and the 2011 March 11 $M_w = 9.0$ Tohoku-Oki earthquake (Miyazaki *et al.* 2011) triggered strong post-seismic deformation at site MCIL. To avoid complications introduced by their post-seismic deformations, we estimated the velocities at those five sites solely from the observations that preceded these earthquakes.

Uncertainties in all of the site velocities are estimated using the method of Mao *et al.* (1999), which uses information about the length of a station time-series and the magnitudes of its white, flicker and random walk noise to estimate realistic site velocity uncertainties. Estimates for the magnitudes of white and flicker noise are taken from our post-processing software. We assume that random walk noise averages 1 mm $(\sqrt{\text{yr}})^{-1}$ at all the sites.

3.2 Clarion and Guadalupe Island coordinate time-series

Fig. 3 shows the daily 3-D station position estimates for the Clarion Island GPS site for 1997–2013 reduced by the motion of the Pacific Plate. The four site occupations are consistent with linear station

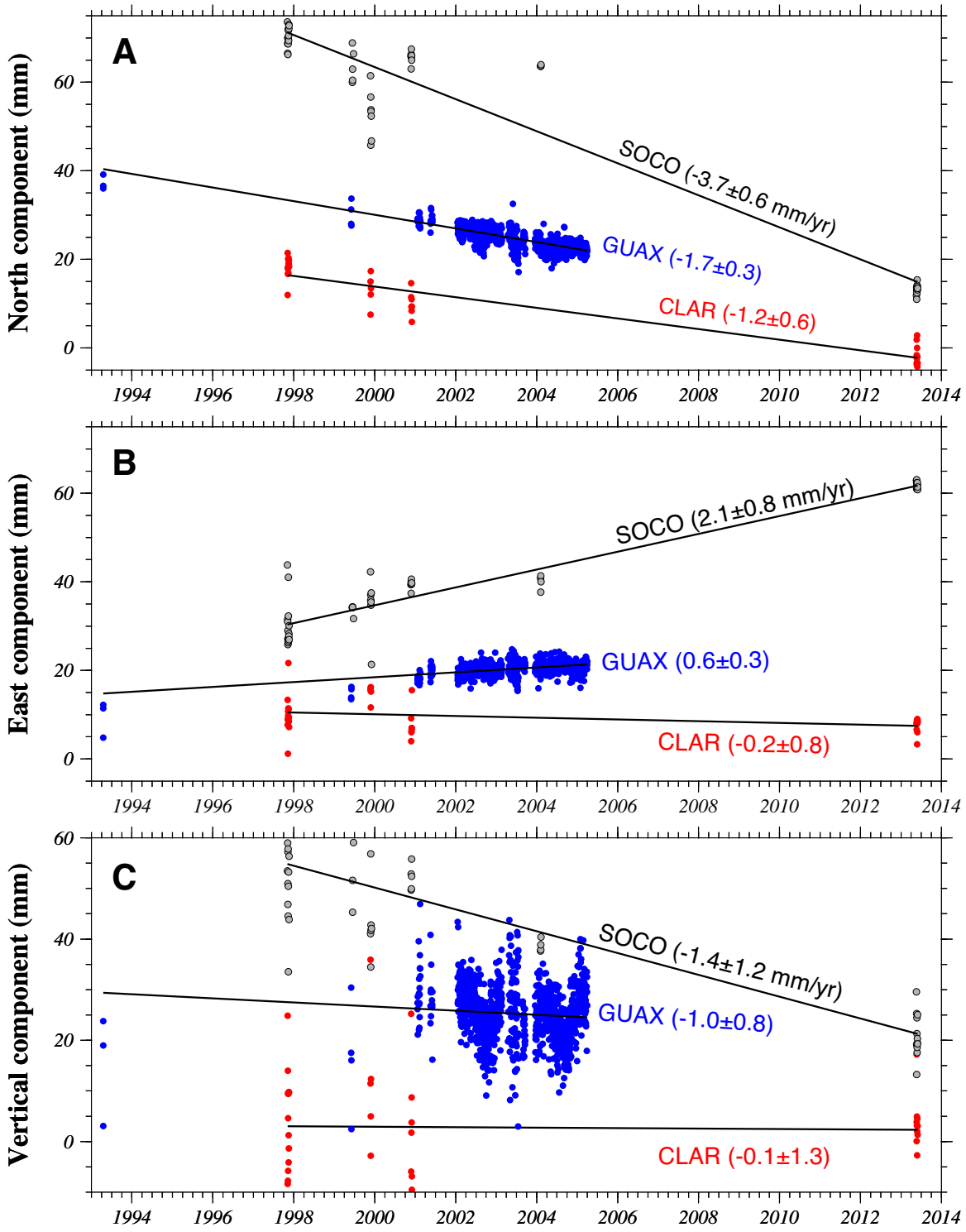

Figure 3. Evolution of daily 3-D positions, 1993–2013, for GPS sites CLAR, GUAX and SOCO on Clarion, Socorro and Guadalupe islands, respectively. Changes in the site latitudes (a) and longitudes (b) are reduced by the motion of the Pacific Plate predicted at each site location (see text), leaving only the movement of each site relative to the plate interior. Panel (c) shows variations in the site elevations. Circles indicate the site positions estimated from 24 hr or less of GPS observations. Solid lines show the slopes that best fit each station's coordinate time-series. The best-fitting site rates and their 1σ uncertainties, both in units of millimetres per year, are listed within parentheses.

motion and reveal 15 mm of southward movement relative to the plate interior during the 15.6 yr spanned by the data (Fig. 3a). Due to the long period spanned by the data and the presence of only 2 and 3 mm of scatter in the east and north components of the daily site positions, the estimated 1σ site velocity uncertainties are relatively small, ± 0.6 and ± 0.8 mm yr^{-1} in the north and east components, respectively (Table 1). The site elevations we estimated for each of the four occupations are remarkably consistent (Fig. 3c), indicating

that our antenna height measurements were reliable and that the antenna phase centres were modelled correctly. By implication, the estimated horizontal components for the station location are also reliable. No significant vertical movement occurred between 1997 and 2013.

The daily positions of the well-behaved GPS sites GAIR/GUAX on Guadalupe island change linearly during the 12 yr spanned by the observations (Fig. 3) and are scattered by only 1.3 and 1.1 mm in their north and east components relative to the monthly average positions. The site velocity uncertainties, ± 0.4 and ± 0.3 mm yr^{-1} in the north and east components, respectively (Table 1), are smaller than the velocity uncertainties for the campaign site on Clarion Island site, as expected given that the site on Guadalupe Island ran continuously for $\sim$3 yr.

3.3 Socorro Island coordinate time-series and volcanic deformation

Between 1997 and 2013, the GPS site SOCO on Socorro Island moved 55 mm to the south and 30 mm to the east relative to the Pacific Plate interior (red circles in Fig. 3), several times more than was measured at nearby Clarion Island during the same 15.6-yr-long period. The site elevations record slow subsidence of the site during the same period (Fig. 3c), similar to the vertical motion measured at a nearby DORIS site (Fig. 4c).

From weekly DORIS measurements between early 1990 and mid 2005 at a beacon located only 750 m from GPS site SOCO, Briole *et al.* (2009) conclude that the motion of the DORIS beacon is strongly influenced by volcanic deformation associated with the Socorro Island shield volcano. In particular, after correcting the motion of the DORIS beacon for movement of the Pacific Plate, Briole *et al.* (2009) find that the DORIS beacon moved $\approx$300 mm to the northwest and subsided by $\approx$300 mm between 1993 and 1996, during a 3-yr-long submarine eruption that was focused $\sim$15 km northwest of the beacon (see inset to Fig. 4). Between 1996 and 2002, the DORIS monument reversed its motion and moved directly away from the 1993–1996 submarine eruption (red arrow in map inset of Fig. 4). Briole *et al.* (2009) interpret this as evidence for re-inflation of the magma chamber that was vacated by the 1993–1996 eruption.

In late September of 2002, the DORIS weekly solutions reveal a sudden, ESE-directed $\approx$100 mm horizontal offset (Fig. 4) that was not associated with an earthquake, a known eruption, or any change in hardware at the site (Briole *et al.* 2009). The offset initiated another reversal in the direction of site motion, such that the DORIS beacon began moving back towards the 1993–1996 eruption centre (Fig. 4). Although the observations reported by Briole *et al.* (2009) end in mid 2005, we procured and augmented their time-series with additional weekly solutions that continued until the beacon failed in late 2009 (http://ids-doris.org and Willis *et al.* 2010). The updated position time-series shows a steady continuation of the motion measured after the offset in September of 2002, consisting of slow subsidence (Fig. 4c) and horizontal motion towards N65°W (blue arrow in map inset of Fig. 4). We interpret the slow subsidence and movement of the DORIS beacon towards the eruption center during this period as evidence for deflation of the magma chamber or possible viscoleastic deformation associated with the 1993–1996 eruption.

Although our GPS measurements at SOCO are too infrequent to detect the transient deformation that is indicated by the weekly DORIS solutions (Fig. 4), the SOCO position time-series is nonetheless consistent to first-order with the deformation measured by the nearby DORIS beacon. We thus infer that the GPS site is also influenced by discharge and recharge of magma beneath the shield volcano and exclude measurements from SOCO from our ensuing analysis of plate-scale deformation.

4 RESULTS

Our analysis is presented in multiple stages. We first invert the velocities of all 26 GPS sites from the central, southern and western areas of the Pacific Plate to find their best-fitting angular velocity and evaluate the residual velocity field for evidence of possible distributed deformation within the Pacific Plate. We then determine the motions of Clarion and Guadalupe islands relative to the newly defined Pacific Plate reference frame and test five hypotheses for their apparently significant motions. Three of these postulate that the slow movements of the two sites are artifacts of possible errors in our estimate of the Pacific Plate angular velocity due to possible slow drift of Earth's geocentre in ITRF08, small but cumulative elastic offsets from large-magnitude earthquakes around the Pacific rim (Tregoning *et al.* 2013), or viscoelastic deformation triggered by large-magnitude earthquakes within and near the Pacific basin since 1950 (Pollitz *et al.* 1998). We also test whether elastic plate deformation due to locked plate boundary faults in the Gulf of California or distributed tectonic deformation across some or all of the several thousand km of oceanic lithosphere that separates the two islands from the rest of the Pacific Plate might explain the slow motions of Clarion and Guadalupe Islands.

4.1 Best-fitting angular velocity and residual site motions

Using fitting functions described by Ward (1990), we inverted the velocities and uncertainties for 26 continuous GPS stations from the central, western and southern Pacific Plate to find their best-fitting Pacific Plate angular velocity and its uncertainties (Table 2). The new Pacific-ITRF08 angular velocity fits the station velocities well (Figs 5, 6, and 7) and confirms the good fits reported by previous authors from earlier realizations of the Pacific Plate velocity field (e.g. Larson *et al.* 1997; DeMets & Dixon 1999; Beavan *et al.* 2002; Marquez-Azua *et al.* 2004; Plattner *et al.* 2007). The weighted rms misfits for the new angular velocity are 0.44 and 0.41 mm yr^{-1} for the north and east velocity components, respectively, consistent with the average misfits that are suggested by a visual examination of the residual velocities (red arrows in Fig. 7b). The least-squares misfit normalized by the degrees of freedom (i.e. $\chi^2{}_\nu$) is 1.36, indicating that the velocity misfits are 17 per cent larger on average than the estimated velocity uncertainties. Below, we investigate whether any of several possible *a priori* corrections to the 26 site velocities reduces the misfits such that $\chi^2{}_\nu$ is closer to its expected value of 1.0.

Fig. 6 shows the misfits of the new best-fitting angular velocity for all 26 Pacific Plate sites and sites CLAR, GUAX and SOCO as a function of location (Fig. 6a) and seafloor age (Fig. 6b). Excluding the latter three sites, whose misfits are discussed in the following section, only one of the 26 site velocities, that for site CHTI, is misfit by more than 1 mm yr^{-1} (Fig. 7d). An examination of the regional velocity misfits (Figs 7c–f) suggests that Micronesia is the only region where the misfits exhibit a semi-coherent pattern (Figs 6a and 7f). There, five of the seven velocity misfits, all for sites located on the oldest seafloor in the Pacific, include a northward component (Fig. 7f). As a test, we inverted the velocities from the seven sites in Micronesia separately from 19 velocities for sites elsewhere on

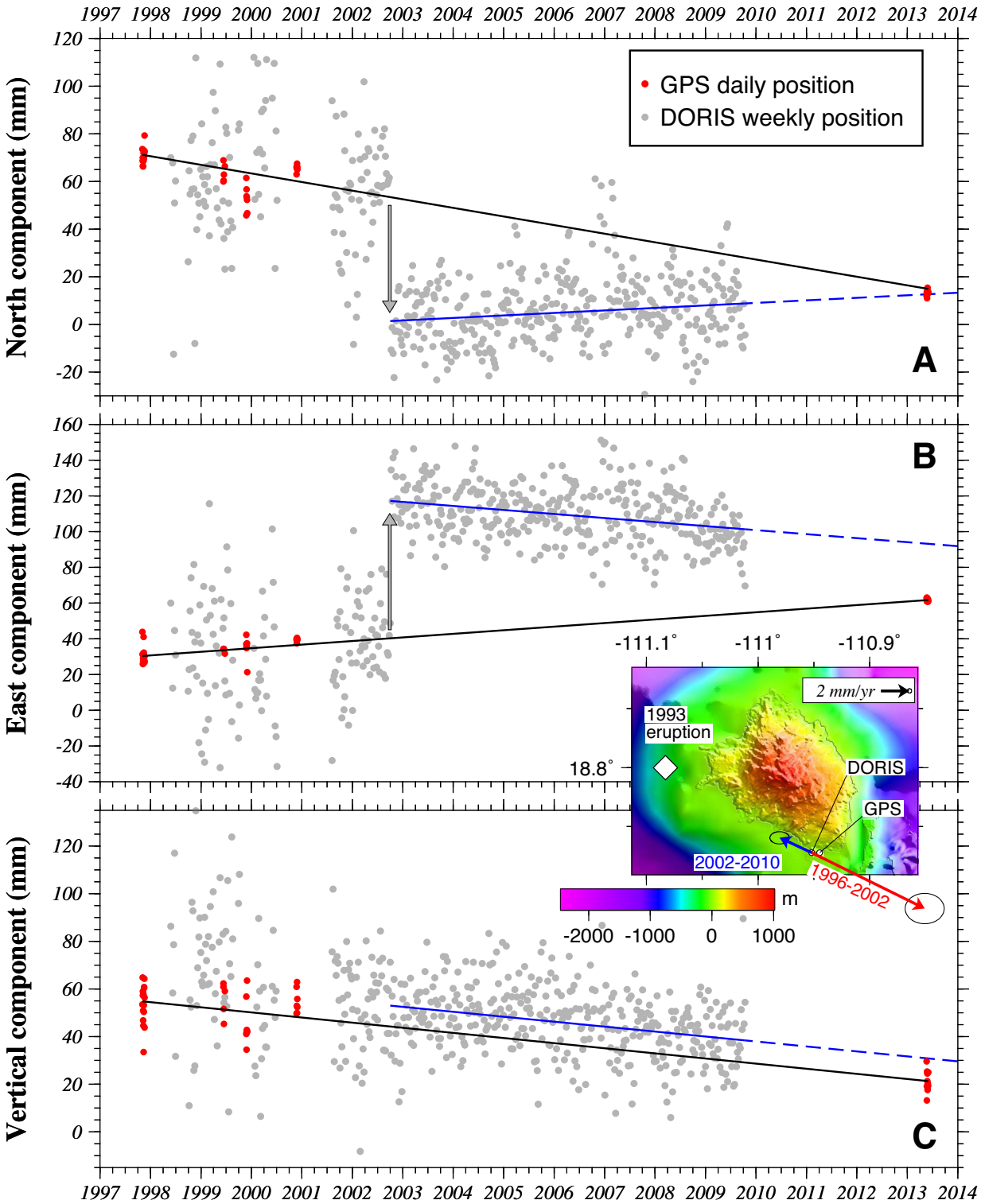

Figure 4. Evolution of daily 3-D positions, 1997–2013, for GPS site SOCO (red circles) and weekly positions for DORIS site SODB (gray circles), both on Socorro Island. Changes in the site latitudes (a) and longitudes (b) are reduced by the motion of the Pacific Plate predicted at each site location. Black lines best fit the GPS station coordinates. Blue lines best fit the weekly DORIS solutions, including a sudden offset in late September of 2002 (marked by the vertical arrows). Inset map of Socorro Island shows the estimated location (diamond) of the 1993–1996 submarine eruption (Briole *et al.* 2009) and-fitting best velocities from 1996 to 10/2002 from Briole *et al.* (2009) and 10/2002 to late 2009 (this study).

the Pacific Plate to find best-fitting angular velocities for each data subset. We then compared the summed, least-squares misfit for the two angular velocities ($\chi^2 = 54.8$) to the misfit for the angular velocity that simultaneously best fits all 26 site velocities ($\chi^2 = 66.7$). The more complex, two-plate model improves the fit at the 97.5 per cent confidence level, which we consider to be marginally significant. The average motion of the seven Micronesian sites with respect to the remainder of the Pacific Plate is 0.6 ± 0.4 mm yr^{-1}

Table 2. Best-fitting Pacific Plate angular velocity.

χ^2_ν	Angular velocity			Covariances					
	ω_x	ω_y	ω_z	σ_{xx}	σ_{yy}	σ_{zz}	σ_{xy}	σ_{xz}	σ_{yz}
1.36	−0.001946	0.005117	−0.010536	5.27	1.32	1.27	0.94	0.08	0.13

Notes: The best-fitting angular velocity specifies Pacific Plate motion relative to ITRF2008 and is determined from 26 of the 29 GPS site velocities from Table 1, excluding the velocities for sites CLAR, GUAX and SOCO. χ^2_ν is the weighted least-squares fit normalized by the degrees of freedom. The Cartesian components of the angular velocity, which have units of radians per Myr, correspond to an angular velocity of 62.544°S, 110.817°E 0.680° per Myr. The covariances, which are propagated linearly from the GPS site velocity uncertainties, have units of 10^{-10} radians^2 per Myr^2.

towards N20°W ± 30° (95 per cent limits). In Sections 4.5 and 4.6, we test whether this slow northward movement might be a regional elastic or viscoelastic response to large historic earthquakes.

Due to the vast area that is spanned by the 26 Pacific Plate site velocities and the small uncertainties in the site velocities, the best-fitting angular velocity is well determined. The small angular velocity covariances (given in Table 2) propagate into formal 1σ uncertainties of only ±0.1 mm yr^{-1} and ±0.1° in the linear velocities that are predicted at most locations in and around the Pacific basin. The formal angular velocity uncertainties almost surely understate the actual uncertainties because they exclude sources of possible systematic biases in the GPS site velocities described later.

4.2 Evidence for anomalous motions of Clarion and Guadalupe islands

Relative to the Pacific Plate, Clarion Island moves 1.2 ± 0.6 mm yr^{-1} towards S09°W ± 38° and Guadalupe Island moves 1.9 ± 0.3 mm yr^{-1} towards S19°E ± 10° (Figs 2 and 7a). GPS site SOCO on Socorro Island moves 4.3 ± 0.7 mm yr^{-1} towards S29°E ± 10° relative to the plate interior (Fig. 2), more rapidly than but in the same direction as the sites at CLAR and GUAX. Evidence described in Section 3.3 indicates that SOCO's motion is affected by volcanic deformation; its velocity is thus discounted in the analysis later.

We evaluated the statistical significance of the motions of Clarion and Guadalupe islands relative to the plate interior via an *F*-ratio comparison of the fits of one-plate and two-plate models (Stein & Gordon 1984) to the velocities for the 26 Pacific Plate sites and CLAR and GUAX. We first jointly inverted the velocities of CLAR, GUAX and the 26 Pacific Plate sites to find their best-fitting angular velocity and its weighted least-squares misfit ($\chi^2 = 100.0$). We then inverted the two velocity subsets separately to find their best-fitting angular velocities and summed misfit ($\chi^2 = 67.9$). A comparison of the two misfits using the *F*-ratio test gives $F = 7.9$. For 3 degrees of freedom versus 50 degrees of freedom, the probability is only 0.002 per cent that the superior fit of the two-plate model is a random outcome of fitting the observations with 3 additional parameters. The motions of Clarion and Guadalupe islands relative to the Pacific Plate are thus significant at the 99.99 per cent confidence level. We note that the velocities of the two sites are estimated from GPS measurements that were made at different times and at locations that are separated by 1225 km. It therefore seems unlikely that the motions of both sites relative to the plate interior could be an artifact of correlated errors in their estimated velocities due to correlations in one or more of the various sources of noise that can affect estimates of GPS station positions.

As an extra precaution, we tested how the uncertainties that we assigned to the velocities for sites CLAR and GUAX influence the significance level of their apparent motions relative to the Pacific Plate. In general, the velocity uncertainty for a site with a long time-series (such as sites CLAR and GUAX) depends primarily on the magnitude of the random-walk noise that affects its position time-series (Mao *et al.* 1999). As a test, we doubled to 2 mm $(\sqrt{\text{yr}})^{-1}$ the random-walk noise that we assumed when estimating uncertainties for sites CLAR and GUAX. This roughly doubled their estimated velocity uncertainties. We then repeated the one- versus two-plate test described in the previous paragraph. Even with these more conservative uncertainties, the two-plate model improves on the fit of the one-plate model at the 99 per cent confidence level. The motions of sites CLAR and GUAX relative to the plate interior are thus still statistically significant even if more pessimistic uncertainties are assigned to both site velocities.

The slow southward motions of sites CLAR and GUAX relative to the plate interior are unexpected given that both islands should be relatively immune to earthquake cycle effects and distributed deformation associated with the Pacific–North America Plate boundary, which is ∼450 km or more east of the islands. Although GPS sites in the nearby Baja California peninsula also move slowly to the SSE-to-SE (e.g. sites LPAZ and MSD1 in Fig. 2), their motions are more easily attributed to detachment of the Baja sliver Plate from the Pacific Plate and complexities associated with nearby plate boundary faults (Dixon *et al.* 2000; Plattner *et al.* 2007).

We next test a series of hypotheses for the slow motions of sites CLAR and GUAX relative to the plate interior.

4.3 Effect of unmodelled geocentral translations

All realizations of the international terrestrial reference frame (ITRF) include uncertainties in the motion of Earth's centre of mass (Argus 1996; Heki 1996), such that every realization of ITRF suffers from some drift of Earth's origin that maps one-to-one into systematic biases in GPS site velocities. For example, a hypothetical 1 mm yr^{-1} drift of Earth's origin along the positive *Z*-axis would impart a ≈1 mm yr^{-1} vertical (upward) bias to geodetic sites at high northern latitudes and a systematic ≈1 mm yr^{-1} north-directed bias in the velocities of GPS sites at or near the equator. For large plates such as the Pacific Plate, these location-dependent biases in GPS site velocities may degrade estimates of plate angular velocities and give rise to apparent internal plate deformation where none exists.

Realizations of ITRF are designed in part to minimize drift of Earth's origin (e.g. Altamimi *et al.* 2002). For example, from a simultaneous inversion of geodetic, gravity, and ocean bottom pressure observations, Wu *et al.* (2011) estimate that origin drift in ITRF08, the geodetic frame of reference used in this study, is −0.4 ± 0.1, −0.2 ± 0.1 and −0.5 ± 0.2 mm yr^{-1} in the *X*, *Y* and *Z* directions, respectively. Although these are small in relation to tectonic plate motions of tens of millimetres per year or more, they are large

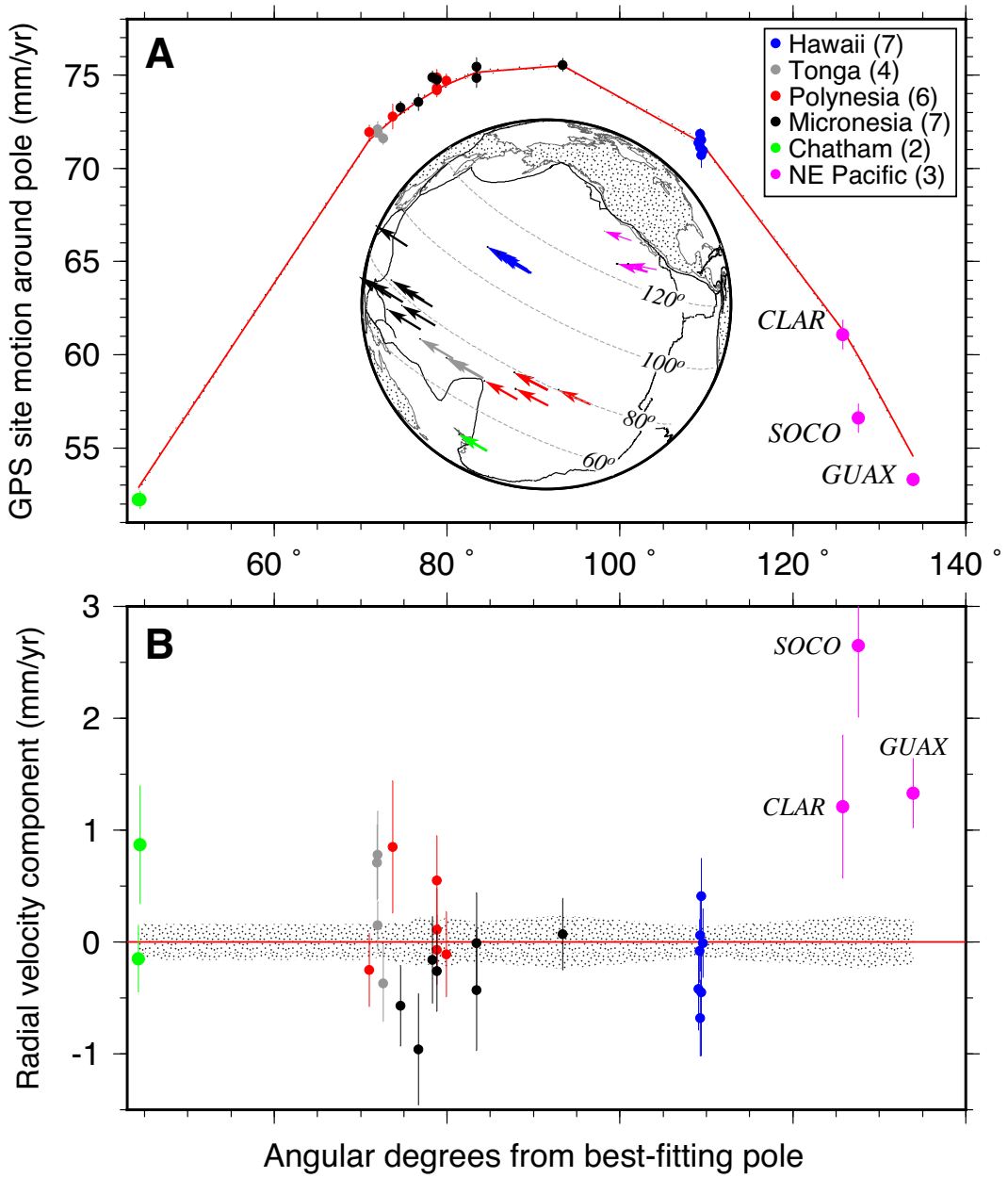

Figure 5. Observed (circles) and predicted (red lines) velocities at Pacific Plate GPS sites relative to ITRF08. Predicted velocities are from the best-fitting angular velocity in Table 2, which is determined from 26 of the 29 GPS site velocities in Table 1 excluding only the velocities of sites CLAR, GUAX and SOCO in the eastern Pacific. The colour coding indicated in the legend defines geographic site groupings that are used in the text and later figures. Arrows on the inset globe show the GPS station velocities relative to ITRF08. The dotted lines on the inset globe are small circles that are spaced every 20 angular degrees from the Pacific-ITRF08 rotation pole (Table 2); these define the angular distances that are indicated on the horizontal axes of (a) and (b). (a) Component of GPS site motion parallel to the small circles around the best-fitting pole (the tangential component). (b) Radial component of GPS site motion, defined as the component of a site's motion towards (negative values) or away from the pole. Vertical bars in (a) and (b) show the 1σ site velocity uncertainties. Shaded areas show the 95 per cent velocity prediction uncertainties.

enough to potentially affect our interpretation of the movements of Clarion and Guadalupe islands, which are only 1–2 mm yr^{-1} relative to the Pacific Plate interior.

We therefore tested whether some or possibly all of the slow southward motions of sites CLAR and GUAX relative to the plate interior might be artifacts of possible drift of Earth's origin in ITRF08. We corrected the Cartesian velocity components of all 28 Pacific Plate GPS sites, including CLAR and GUAX, by the ITRF08 origin drift values estimated by Wu *et al.* (2011). We then inverted 26 of the 28 modified station velocities (excluding CLAR and GUAX) to estimate a new angular velocity for the Pacific Plate. The least-squares misfit for the 26 modified velocities, $\chi^2 = 65.3$, is modestly smaller than for the 26 unmodified site velocities ($\chi^2 = 66.9$) and the WRMS misfits for the two sets of velocities differ negligibly. With respect to the modified frame of reference, sites CLAR and GUAX move even more rapidly towards the south, at respective rates of 1.6 ± 0.6 and 2.1 ± 0.3 mm yr^{-1}, than was previously the case. The Wu *et al.* corrections thus strengthen the evidence for significant motions of CLAR and GUAX relative to the plate interior.

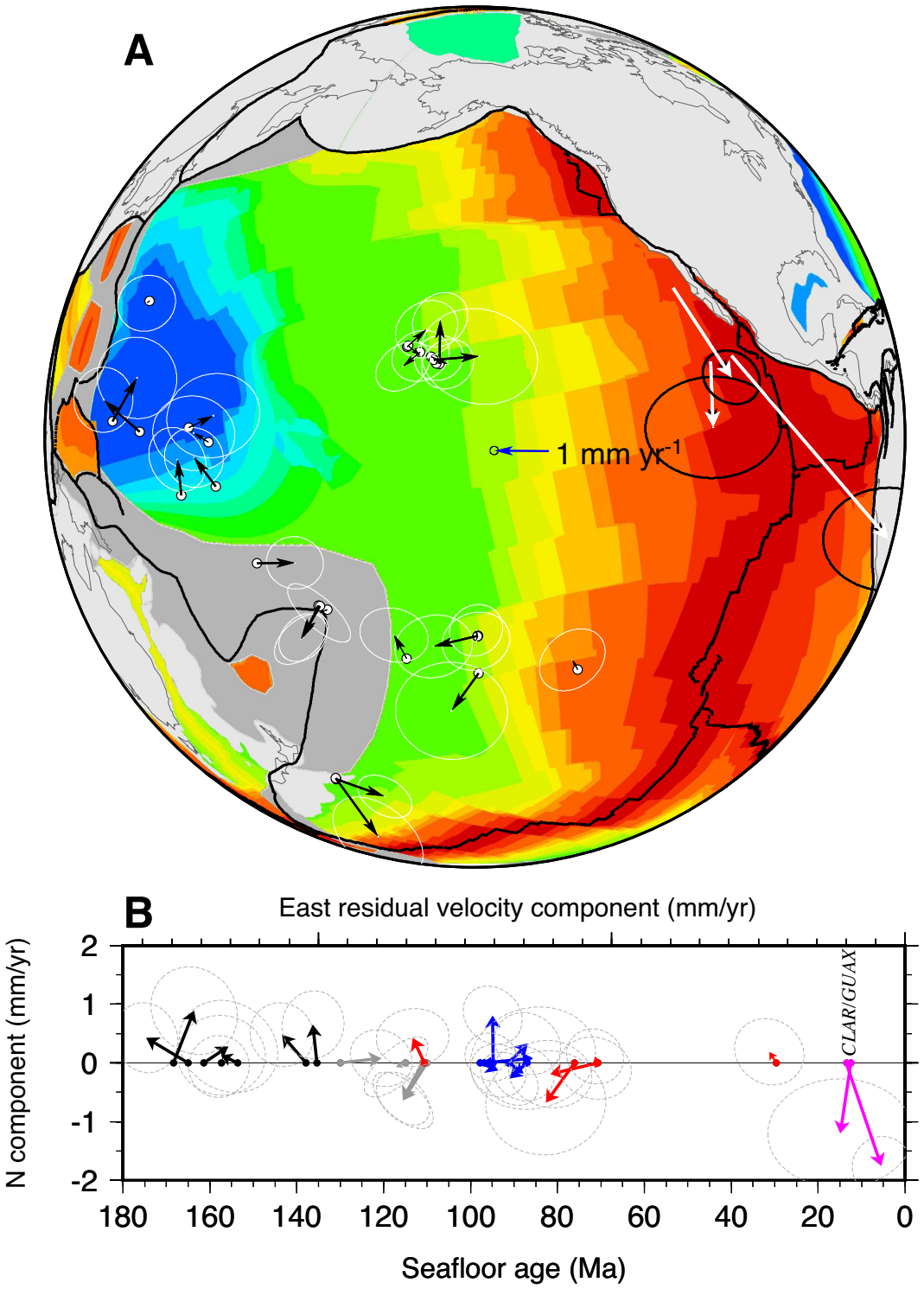

Figure 6. (a) Residual GPS site velocities determined by subtracting the Pacific Plate velocity predicted at each site (Table 2) from the observed station velocity in ITRF08 (Table 1). Black arrows show residual velocities for the 26 GPS stations that were used to estimate the best-fitting Pacific Plate angular velocity in Table 2. White arrows show the residual motions of the Clarion, Guadalupe, and Socorro Island GPS sites. Ellipses show the 2-D, 1σ velocity uncertainties. The seafloor age colour scale is shown in Fig. 1. (b) Residual motions of Pacific Plate sites from (a) as a function of the age of the seafloor on which each GPS site is situated. Dotted ellipses show the 2-D, 1σ uncertainties. Arrow are colour coded based on geographic groupings defined in the legend to Fig. 5(a).

We also evaluated a range of other estimates for origin drift in ITRF08 to determine whether any reduces the misfit to the 26 Pacific Plate velocities and reduces or eliminates the apparent motions of sites CLAR and GUAX. Inversions of the 26 Pacific Plate GPS station velocities using all possible permutations of hypothetical origin drift values between -1.0 and 1.0 mm yr^{-1} for the *X*-, *Y*- and *Z*-axes failed to produce any combination of assumed drift values that significantly reduces both the residual velocities of CLAR and

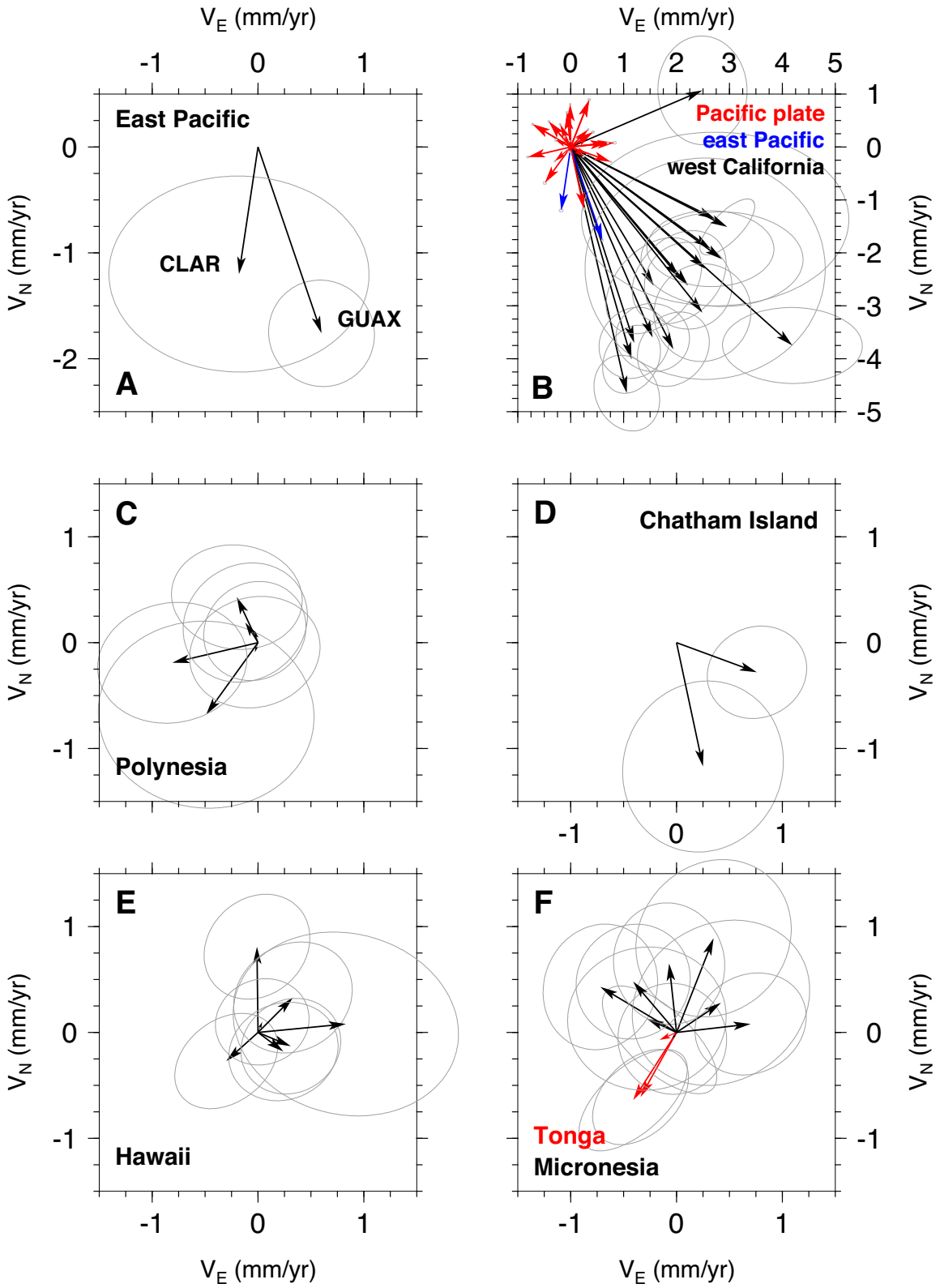

Figure 7. Motions of GPS sites by geographic location as defined in the legend for Fig. 6(a) reduced by the motion of the Pacific Plate relative to ITRF08 (Table 2). (a) Residual velocities of sites CLAR and GUAX in the eastern Pacific. (b) Residual motions of all 26 Pacific Plate sites (red), sites CLAR and GUAX (blue), and 17 GPS stations from western California outboard from the creeping and transitional segments of the San Andreas fault (black). (c–f) Residual velocities by geographic location of the 26 stations that were used to estimate the Pacific Plate angular velocity in Table 2 (also see Fig. 6). Error ellipses are 2-D, 1σ.

GUAX and the least-squares misfit to the 26 Pacific Plate GPS station velocities.

We conclude that the movements of Clarion, Guadalupe or Socorro islands relative to the Pacific Plate are not artifacts of possible drift of Earth's origin in ITRF08.

4.4 Interseismic elastic effects of faults in the Gulf of California

We next tested whether elastic deformation due to interseismic coupling of Pacific–North America Plate boundary faults ≈450 km or more east of Guadalupe and Clarion islands may affect the motions of the two islands. We constructed a homogeneous elastic half-space model in which we embedded vertical strike-slip faults that reproduce the geometry of the Pacific–North America Plate boundary in the Gulf of California and southern California (23°–35°N). For a long-term fault slip rate of 48 mm yr^{-1} (DeMets *et al.* 2010) and assumed fault locking depth of 10 km, the half-space model predicts a southeast-directed elastic slip deficit of 0.2 mm yr^{-1} at Guadalupe Island and a slip deficit less than 0.1 mm yr^{-1} at Clarion Island, both relative to the Pacific Plate. Increasing the prescribed fault locking depth to 20 km increases the predicted elastic slip deficit at GUAX to 0.3 mm yr^{-1}.

The predicted elastic slip deficits are too small to explain the observed southward motions of Guadalupe and Clarion islands, although elastic deformation could be responsible for as much as 0.3 mm yr^{-1} of the 1.9 ± 0.3 mm yr^{-1} motion observed at GUAX.

4.5 Coseismic elastic effects of large-magnitude Pacific basin earthquakes

Tregoning *et al.* (2013) propose that the cumulative effects of large earthquakes in the Indian Ocean and Pacific basin may degrade velocity estimates at distant GPS sites by enough to influence the realization of a plate reference frame, even if the offset caused by any one earthquake is too small to detect within the noise that is typical of most continuous GPS position time-series. From forward calculations of the elastic offsets that were caused by seventeen M_w >8 earthquakes since 2000, they demonstrate that those earthquakes have perturbed GPS site velocities across most of Earth's surface by 0.1–0.3 mm yr^{-1}, including locations throughout the Pacific basin.

If Tregoning *et al.*'s hypothesis is correct, then the velocities we estimate for some or possibly all of the 29 Pacific Plate GPS stations that are used in this study are biased to varying degrees by coseismic offsets that were ignored while estimating the GPS site velocities. It follows that correcting the position time-series of the 29 stations for the effects of these earthquakes prior to estimating the site velocities should yield a set of corrected site velocities with a smaller rms scatter relative to the predictions of their best-fitting angular velocity than for the uncorrected site velocities.

We therefore calculated coseismic offsets at all 29 GPS sites listed in Table 1 for all 17 earthquakes that were considered by Tregoning *et al.* (2013) (http://rses.anu.edu.au/geodynamics/Great_earthquake_deformation/) and applied the offsets at each GPS site while re-estimating its best-fitting velocity. Doing so changed the velocities at 26 of the 29 GPS sites by less than 0.1 mm yr^{-1}, too small to affect any of our results. The velocities of only three of the 29 sites changed at levels comparable to their assigned uncertainties, namely, sites ASPA, SAMO and TRUK. The velocities at ASPA and SAMO changed by 0.3 mm yr^{-1} upon correcting their time-series for the coseismic offset from the $M = 8.1$ 09.29.2009 Samoa earthquake. The velocity for TRUK changed by 0.4 mm yr^{-1} due to coseismic offsets from the $M = 8.0$ 2000 November 16 New Ireland earthquake and the $M = 9.3$ 2004 December 26 Sumatra earthquake. Our results validate Tregoning *et al.*'s assertion that individual site velocities may be affected at levels close to their assigned uncertainties.

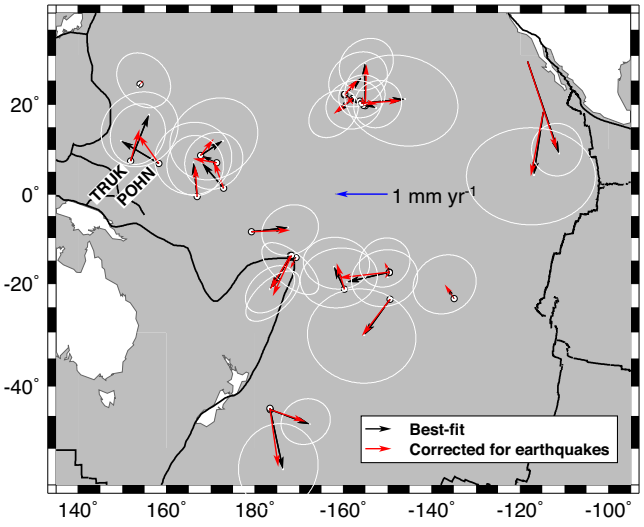

Figure 8. Comparison of velocity misfits from an inversion of Pacific Plate GPS site velocities that were derived from coordinate time-series that were corrected for calculated offsets from $M \geq 8$ Pacific basin earthquakes (red arrows) and misfits for the best-fitting Pacific Plate angular velocity (black arrows) from Table 2. Further details are given in Section 4.5.

An inversion of the corrected velocities for the 26 Pacific Plate sites gives reduced chi-square (χ^2_ν) of 1.33, corresponding to WRMS misfits of 0.45 and 0.39 mm yr^{-1} for the north and east velocity components, respectively. For comparison, our inversion of the uncorrected velocities (Section 4.1) gives χ^2_ν of 1.36 and respective north and east WRMS velocity misfits of 0.44 and 0.41 mm yr^{-1}. A visual comparison of the residual fits for the original and offset-corrected velocities (red and black arrows in Fig. 8, respectively) shows that the principal improvements in fit are at sites POHN and TRUK in Micronesia, where the fits improved by 0.2 and 0.3 mm yr^{-1}, respectively. In Micronesia, where the original residual site velocities include a slow but significant northward component of motion (Section 4.1 and Fig. 7f), the modified residual velocities (red arrows in Fig. 8) still include a significant northward component, albeit at a modestly lower significance level (94.8 per cent) than was the case for the uncorrected velocities (97.5 per cent).

The improvement in fit upon correcting the GPS velocity field for the effects of distant earthquakes, though small, validates the concept that coseismic effects of distant earthquakes that are too small to discriminate from the noise in GPS coordinate time-series can nonetheless have a cumulative effect that is large enough to warrant *a priori* corrections to GPS coordinate time-series.

In a Pacific Plate frame of reference that is defined by an inversion of the 26 site velocities that are corrected for earthquake offsets, the GPS sites on Clarion and Guadalupe islands move 1.2 ± 0.6 mm yr^{-1} towards S11°W ± 37° and 1.8 ± 0.3 mm yr^{-1} towards S18°E ± 10°. These differ insignificantly from the residual velocities that were determined without any corrections for earthquake offsets (compare red and black arrows at Clarion and Guadalupe Islands in Fig. 8). The southward motions of the two islands relative

to the plate interior are thus robust with respect to corrections for the elastic effects of large earthquakes.

4.6 Viscoelastic effects of large-magnitude earthquakes from 1950 to present

Pollitz *et al.* (1998) propose that a series of large subduction earthquakes between 1952 and 1965 along the Alaska, Aleutian and Kuril-Kamchatka trenches triggered viscoelastic relaxation of the asthenosphere below the Pacific Plate, resulting in transient deformation as fast as several millimetres per year until at least the late 1980s throughout much of the Pacific and Arctic basins. To test their hypothesis, Pollitz *et al.* used rupture locations and slip solutions for twelve large-magnitude Pacific basin earthquakes between 1952 and 1986 to predict the evolution of viscoelastic deformation in the Pacific and Arctic basins through the mid-1990s. They concluded that a viscosity of 5×10^{17} Pa s for the asthenosphere below the Pacific Plate is the most consistent with the spatiotemporal evolution of seismicity in western North America and the eastern Arctic Basin. In support of this conclusion, they found that correcting the geodetic velocities of sites on four mid-Pacific islands for the viscoelastic deformation corresponding to an asthenospheric viscosity of 5×10^{17} reduced by 75 per cent the variance of those velocities with respect to their best-fitting Pacific Plate angular velocity.

Based on their encouraging results, we investigated whether viscoelastic deformation of the Pacific Plate provides a useful framework for understanding our new GPS velocity field, including the hard-to-explain southward motions of Clarion and Guadalupe islands relative to the plate interior. Between 1950 and early 2014, 40 earthquakes with moment-magnitudes of 8 or larger occurred close enough to the Pacific basin to cause possible viscoelastic deformation within the basin, including five earthquakes with magnitudes equal to or larger than 9 (Table 3 and Fig. 9). We compiled a coseismic slip solution for each earthquake and used Visco-1D (version 3) (Pollitz 1997) to estimate viscoelastic deformation at daily intervals for each earthquake from the time of the earthquake to the present at locations throughout the Pacific basin (including each GPS site in Table 1).

We test Pollitz *et al.*'s hypothesis as follows. If the viscoelastic surface deformation that is predicted for a series of earthquakes and a prescribed mantle viscosity structure is approximately correct, then a well-distributed set of Pacific Plate GPS site velocities that are corrected for the viscoelastic deformation and inverted to find their best-fitting angular velocity should have a smaller WRMS misfit than for the uncorrected GPS site velocities. Several factors complicate such a test. In particular, the mantle viscosity structure and rheological behaviour that are required for the viscoelastic calculation are imperfectly known, as are the earthquake slip solutions, which include the depth, location and extent of a rupture and the direction and magnitude of slip along the fault. The former are important and are discussed in the following section. The latter are less important for our analysis because most of the GPS sites we use are located hundreds to thousands of kilometres from the earthquakes for which we estimate viscoelastic deformation. At these distances, the viscoelastic response is well approximated from the first-order attributes of a coseismic slip solution, including its moment, its rupture location and extent, and its average rake. The viscoelastic effects of local variations in the magnitude and/or rake of slip along the fault plane are attenuated at large distances from an earthquake and can be ignored for this analysis.

4.6.1 Prescribed viscoelastic models

We estimate viscoelastic deformation using the layered 'Rheology 1' viscoelastic structure for oceanic lithosphere and mantle described by Pollitz *et al.* (2006). This consists of an elastic lithosphere from the surface to a depth of 62 km, a Maxwell rheology asthenosphere between depths of 62 and 220 km, and Maxwell-rheology upper and lower mantles with respective viscosities of 10^{20} and 10^{21} Pa s. The top and bottom depths for the asthenosphere correspond approximately to the limits determined from independent analyses of seismic data (Gaherty *et al.* 1996; Tan & Helmberger 2007). The mantle density structure follows that of PREM (Dziewonski & Anderson 1981) and the asthenopheric viscosities that we evaluate (5×10^{17}, 3×10^{18} and 1×10^{19} Pa s) span the viscosity range estimated by Hirth & Kohlstedt (1996) for olivine aggregates in the presence of water at temperatures and pressures in the upper oceanic mantle (see also Pollitz *et al.* 1998).

We do not estimate deformation for two other mantle rheologies, namely, the biviscous Burger body rheology described and used by Pollitz *et al.* (2006) to model transient, near-field deformation after the 2004 Sumatra and 2005 Nias earthquakes or the power-law rheology successfully used to describe transient deformation after the 1992 Landers, 1999 Hector Mine and 2002 Denali earthquakes (Freed & Burgmann 2004; Freed *et al.* 2006; Freed *et al.* 2010). These rheologies are tailored to simulate both the rapid post-seismic deformation that occurs within weeks to years of an earthquake and the slower deformation that persists for years or decades afterwards. In this study, GPS observations that exhibit rapid transient post-seismic deformation are excluded from our data and most of our GPS stations are located thousands of kilometres from seismically active areas (Fig. 9). Our observations are well suited for detecting long-term deformation that should be well approximated by the simpler Maxwell rheology that we employ. They are poorly suited for discriminating between alternative mantle rheologies, which are better tested with observations that are close to a given earthquake in both space and time.

4.6.2 Example: effect of $M_w = 9.2$ 1964 Alaska earthquake

Figs 10(a)–(c) show predictions of the viscoelastic deformation from the 1964 $M = 9.2$ Alaska earthquake, the largest earthquake to occur on a Pacific Plate boundary since 1950, for asthenospheric viscosities of 5×10^{17}, 3×10^{18} and 1×10^{19} Pa s. For convenience, we depict the predicted viscoelastic deformation as velocities averaged over a twenty-year period from 1994 to 2014, spanning most of the period of modern GPS measurements. As expected, the directions of surface deformation at locations south of the 1964 earthquake rupture zone generally point northward towards the rupture zone, representing viscous flow in the mantle (dominantly within the low-viscosity asthenosphere) that relaxes stress that propagated slowly outward from the rupture zone during the years and decades after the earthquake. The predicted velocities range from several millimetres per year for an asthenospheric viscosity η of 5×10^{17} Pa s to less than 0.2 mm yr^{-1} for $\eta = 1 \times 10^{19}$ Pa s.

The black and red arrows in Fig. 10(d), respectively show the original GPS station velocities relative to the Pacific Plate and the same velocities after correcting for the viscoelastic velocity perturbation calculated for the asthenospheric viscosity of 5×10^{17} Pa s (shown in Fig. 10a). The latter velocities were determined in three stages. We first subtracted the daily viscoelastic deformation predicted at each GPS site from each GPS site's observed daily

Table 3. Earthquake information for viscoelastic modelling.

Date (Mo.Dy.Yr)	M_w	M_o (dyne cm)	Lat. (°N)	Long. (°E)	Reference
11.04.1952	9.0	3.5×10^{29}	52.76	160.06	Kanamori (1976)
03.09.1957	8.6	8.8×10^{28}	51.63	−175.41	Johnson & Satake (1993)
11.06.1958	8.4	4.4×10^{28}	44.38	148.58	Fukao & Furumoto (1979)
05.22.1960	9.5	2.0×10^{30}	−38.29	−73.05	Fujii & Satake (2013)
10.13.1963	8.6	7.5×10^{28}	44.5	149.5	Kanamori (1970)
03.27.1964	9.2	7.5×10^{29}	61.0	−147.63	Kanamori (1970)
02.24.1965	8.7	1.4×10^{29}	51.40	179.56	Beck & Christensen (1991)
10.17.1966	8.3	2.9×10^{28}	−10.92	−78.79	Beck & Ruff (1989)
05.16.1968	8.3	2.8×10^{28}	40.84	143.22	Kanamori (1971)
08.11.1969	8.3	2.2×10^{28}	43.18	147.48	Abe (1973)
07.14.1971	8.1	1.2×10^{28}	−5.52	153.90	Schwartz *et al.* (1989)
07.25.1971	8.2	1.8×10^{28}	−4.89	153.18	Schwartz *et al.* (1989)
06.17.1973	7.9	6.7×10^{27}	43.05	145.76	Shimazaki (1974)
10.03.1974	8.1	1.5×10^{28}	−12.39	−77.66	Beck & Ruff (1989)
12.12.1979	8.3	2.9×10^{28}	1.60	−79.36	Beck & Ruff (1984)
03.03.1985	8.1	1.5×10^{28}	−33.14	−71.76	Mendoza *et al.* (1994)
09.19.1985	8.1	1.5×10^{28}	18.18	−102.57	Mendoza & Hartzell (1989)
05.07.1986	8.1	1.3×10^{28}	51.41	−174.83	Hwang & Kanamori (1986)
05.23.1989	8.1	1.4×10^{28}	−52.34	160.57	Velasco *et al.* (1995)
10.04.1994	8.3	2.6×10^{28}	43.37	147.66	Kikuchi & Kanamori (1995)
07.30.1995	8.3	2.4×10^{28}	−23.34	−70.26	Pritchard *et al.* (2002)
10.09.1995	7.9	7.5×10^{27}	19.05	−104.21	Hutton *et al.* (2001)
12.03.1995	8.3	3.1×10^{28}	44.62	149.32	Shao & Ji (1995)[3]
02.17.1996	8.3	2.7×10^{28}	−0.92	136.98	Henry & Das (2002)
11.15.2000	8.1	1.2×10^{28}	−3.99	152.26	Geist & Parsons (2005)
06.23.2001	8.5	6.3×10^{28}	−16.38	−73.50	Pritchard *et al.* (2007)
09.26.2003	8.2	2.2×10^{28}	41.78	144.08	Koketsu *et al.* (2004)
12.23.2004	8.2	2×10^{28}	−49.33	161.42	Tregoning *et al.* (2013)
12.25.2004	9.2	6.5×10^{29}	3.30	95.98	Banerjee *et al.* (2007)
03.28.2005	8.7	1.1×10^{29}	2.05	97.06	Banerjee *et al.* (2007)
05.04.2006	8.0	1.1×10^{28}	−20.09	−174.22	Tang *et al.* (2008)
11.15.2006	8.5	5.0×10^{28}	46.59	153.27	Lay *et al.* (2009)
01.13.2007	8.3	2.6×10^{28}	46.24	154.52	Lay *et al.* (2009)
04.01.2007	8.2	1.9×10^{28}	−8.47	157.04	Furlong *et al.* (2009)
08.15.2007	8.2	1.1×10^{28}	−13.35	−76.51	Sladen *et al.* (2010)
09.12.2007	8.5	5.0×10^{28}	−4.44	101.37	Konca *et al.* (2008)
09.29.2009[1]	8.1	1.4×10^{28}	−15.96	−172.84	Beavan *et al.* (2010)
09.29.2009[2]	8.0	1.0×10^{28}	−15.51	−172.16	Beavan *et al.* (2010)
02.27.2010	8.8	1.7×10^{29}	−36.12	−72.90	Lorito *et al.* (2011)
03.11.2011	9.0	3.8×10^{29}	38.30	142.37	W12/K13[4]

Notes: Columns labelled 'Lat.' and 'Long.' give the earthquake epicentral coordinates. Complete information about the slip solution for each earthquake is found in the supplementary documentation. 1 – Thrust faulting sub-event for the 09.29.2009 Tonga trench earthquake. 2 – Normal faulting subevent for the 09.29.2009 Tonga trench earthquake. 3 – The *Shao and Ji* slip solution is located at http://geol.ucsd.edu/faculty/ji/big_earthquakes/1995/12/smooth/1995kuri.html. 4 - See Wang *et al.* (2012) (W12) and Kyriakopoulos *et al.* (2013) (K13).

positions. We then regressed the modified position time-series to find its best-fitting velocity. Finally, we inverted the modified velocities for all 26 Pacific Plate GPS stations to find their best-fitting angular velocity and its corresponding misfits (i.e. the residual GPS site velocities). Correcting the present-day GPS velocity field for the viscoelastic effect of the 1964 Alaska earthquake assuming an asthenospheric viscosity of 5×10^{17} Pa s increases the WRMS misfit to 0.97 mm yr^{-1} relative to that for the original GPS velocities (0.60 mm yr^{-1}) and increases the apparent southward motions of sites CLAR and GUAX relative to the plate interior. The correction thus makes the velocity field more inconsistent.

We next expand the analysis to all 40 earthquakes in Table 3 in order to test rigorously whether the Pacific Plate velocity field contains resolvable information about viscoelastic deformation and whether some or all of the southward motions of the GPS sites on Clarion and Guadalupe islands is attributable to viscoelastic deformation,

4.6.3 Summed viscoelastic effects

Fig. 11 shows the cumulative viscoelastic deformation averaged between 1994 and 2014 for three assumed asthenospheric viscosities and two possible groupings of the 40 earthquakes. One group consists of all 25 earthquakes that occurred on the boundaries of the Pacific Plate. By definition, the stress pulses that migrate towards the plate interior from these earthquakes neither pass through any mantle beneath a mid-ocean ridge nor encounter a subducting slab. They should thus be relatively unaffected by any

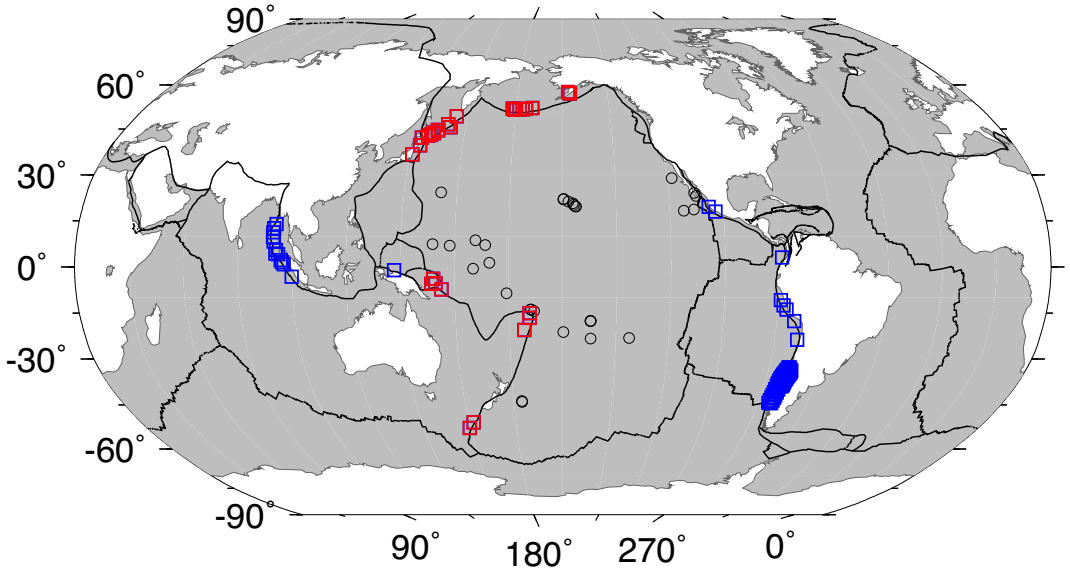

Figure 9. Locations of all 280 fault patches (blue and red squares) that are used to estimate the viscoelastic deformation shown in Figs 11(b), (d) and (f). Red symbols show the fault patches that were used to determine net viscoelastic deformation from earthquakes along only the Pacific Plate boundaries (Figs 11a, c and e). Black circles show locations of GPS sites from Fig. 1. Further information about the earthquakes is given in Table 3.

variations or discontinuities in the viscoelastic mantle that are related to these features. The second group consists of all 40 earthquakes in Table 3, including 15 earthquakes that occurred in the Indian Ocean, the far western Pacific, or along the Peru-Chile trench and Mexico subduction zone. The stress pulses that migrated outward from those earthquakes encountered one or more subducting slabs or the mantle below the East Pacific Rise, with unknown effects on the viscoelastic response.

The globes in the left- and right-hand columns of Fig. 11, respectively show the cumulative viscoelastic deformation for the earthquakes from these two groups. The predicted deformation patterns are sensitive to both the assumed viscosity of the asthenosphere and the group of earthquakes that are used for the calculation. For example, for earthquakes only from the Pacific Plate boundaries, the deformation velocities that are predicted for an asthenospheric viscosity of 5×10^{17} Pa s (Fig. 11a) range from 2 to 5 mm yr^{-1} and point dominantly to the NNW. These reflect the large cumulative moment release of the 1964 Alaska earthquake and additional effects of large-magnitude Aleutian, Kamchatka, and Kuril trench earthquakes since the 1950s (Pollitz *et al.* 1998). In contrast, the deformation pattern for all 40 earthquakes varies significantly with location, particularly for an asthenospheric viscosity of 5×10^{17} Pa s (Fig. 11b). Viscoelastic deformation in the southeastern Pacific is dominated by eastward relaxation towards the $M_w = 9.5$ 1960 Chile earthquake, whereas deformation in the central and western Pacific is a complex superposition of the viscoelastic effects of the 1964 Alaska earthquake, the large Aleutian-Kuril-Kamchatka earthquakes in the 1950s and 1960s, and the more recent 2004 $M_w = 9.2$ Sumatra and 2011 $M_w = 9.0$ Tohuku earthquakes.

As expected, much slower deformation is predicted for higher viscosities of $\eta = 3 \times 10^{18}$ Pa s (Figs 11c and d) and $\eta = 1 \times 10^{19}$ Pa s (Figs 11e and f) than by the lowest viscosity model. The higher viscosity models also predict a different deformation pattern. At higher viscosities, the predicted deformation is determined mainly by the summed viscoelastic responses for the 1960 Chile and 1964 Alaska earthquakes, whereas the deformation attributable to the more recent 2004 Sumatra and 2011 Tohuku earthquakes is still small as of mid 2014. In contrast, all of the largest earthquakes contribute significantly to the cumulative deformation for the lowest viscosity model because of the more rapid asthenospheric viscoelastic response. Interestingly, the predicted relaxation directions for the two highest viscosity models are nearly orthogonal for the two groups of earthquakes (compare panels C to D and E to F in Fig. 11). Sufficiently accurate geodetic observations might eventually discriminate between these two possibilities.

4.6.4 *Tests of proposed models*

We tested the consistency of each of the six viscoelastic models depicted in Fig. 11 with the Pacific Plate GPS velocity field as follows. For each of the six models, we subtracted the daily deformation predicted by the relevant viscoelastic model from the daily GPS position time-series for each of the Pacific Plate GPS sites. We then determined a new, best-fitting site velocity for each corrected GPS position time-series and inverted the corrected site velocities to find their best-fitting Pacific Plate angular velocity. Finally, we compared the least-squares misfit for each model to the misfit for the 26 original Pacific Plate GPS velocities (Fig. 12).

Both models that correspond to asthenospheric viscosities of 5×10^{17} Pa s fit the velocities poorly. Values of χ^2_ν from inversions of the GPS velocities that were either modified for the effects of all 40 earthquakes or for the 25 Pacific basin earthquakes are 16.6 and 9.4, respectively, corresponding to respective weighted rms misfits of 2.8 and 1.5 mm yr^{-1}. For comparison, χ^2_ν and WRMS from the inversion of the 26 original GPS site velocities are 1.36 and 0.60 mm yr^{-1}, respectively. The increases in the least-squares misfits for both models are significant at confidence levels far above 99.99 per cent.

For an assumed viscosity of 3×10^{18} Pa s, the WRMS misfits for both groups of earthquake are 50 per cent higher than the WRMS misfit to the original 26 site velocities (Figs 12a,b,f). The degradation in the fits is most apparent at the GPS sites in the western

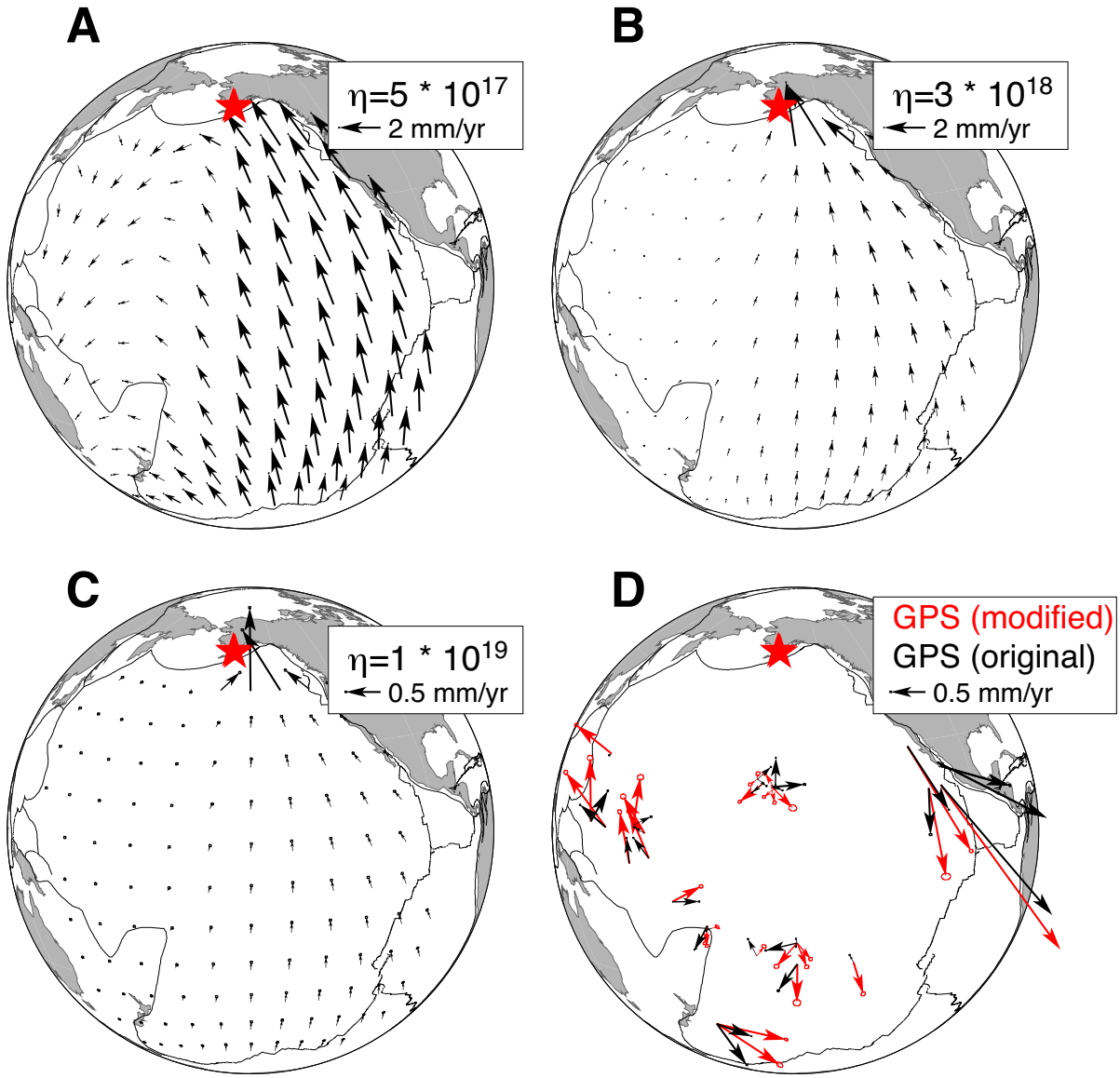

Figure 10. Average velocities from 1994 to 2014 for the horizontal viscoelastic deformation triggered by the $M = 9.0$ 1964 Alaska earthquake for assumed asthenospheric viscosities of (a) 5×10^{17} Pa s, (b) 3×10^{18} Pa s and (c) 1×10^{19} Pa s. Frame of reference is an undeforming Pacific Plate interior. (d) Velocities of GPS sites relative to the Pacific Plate absent any correction for assumed viscoelastic deformation (black arrows – also see Fig. 6) and after correcting for transient viscoelastic deformation from the 1964 Alaska earthquake predicted for an assumed asthenospheric viscosity of 5×10^{17} Pa s (red arrows). Sections 4.6.1 and 4.6.2 describe in more detail the prescribed viscosity structure and the method for correcting the GPS coordinate time-series for the predicted viscoelastic deformation.

Pacific, where the viscoelastic corrections introduce velocity field inconsistencies that were not present in the original velocity field (compare Figs 12a and b to Fig. 12e). In addition, the motions of Clarion and Guadalupe Islands relative to the plate interior are also faster than for the original velocity field. The increases in misfit associated with both models are significant at levels much greater than 99.99 per cent.

For an assigned viscosity of 1×10^{19} Pa s, the misfits to the Pacific Plate site velocities are also larger than for the unmodified velocity field (Figs 12c, d and f), but are smaller than the misfits associated with the lower viscosity of 3×10^{18} Pa s (Fig. 12f). The small differences between the fits for the unmodified velocities and those modified assuming an asthenospheric viscosity of 1×10^{19} Pa s (Fig. 12f) are unsurprising given the slow viscoelastic deformation rates that are predicted for this viscosity (Figs 11e and f).

We conclude that our new Pacific Plate GPS velocity field is highly inconsistent with a long-term asthenospheric viscosity as low as 5×10^{17} Pa s and is also inconsistent with an assumed viscosity of 3×10^{18} Pa s. That the WRMS misfit to the original, unmodified GPS velocity field becomes worse upon applying the velocity field corrections for any of the three asthenospheric viscosities described above suggests that the long-term viscosity of the asthenosphere below the Pacific Plate is higher than 1×10^{19} Pa s. This agrees well with an independent estimate of $\sim 10^{19}$ Pa s for the viscosity of oceanic asthenosphere based on fitting of depth anomalies along the East Pacific Rise and Australia–Antarctic Discordance (Buck *et al.* 2009). Both argue against the existence of long-term, long-wavelength viscoelastic perturbations of geodetic velocity fields in oceanic regions, at least at levels presently detectable with GPS measurements.

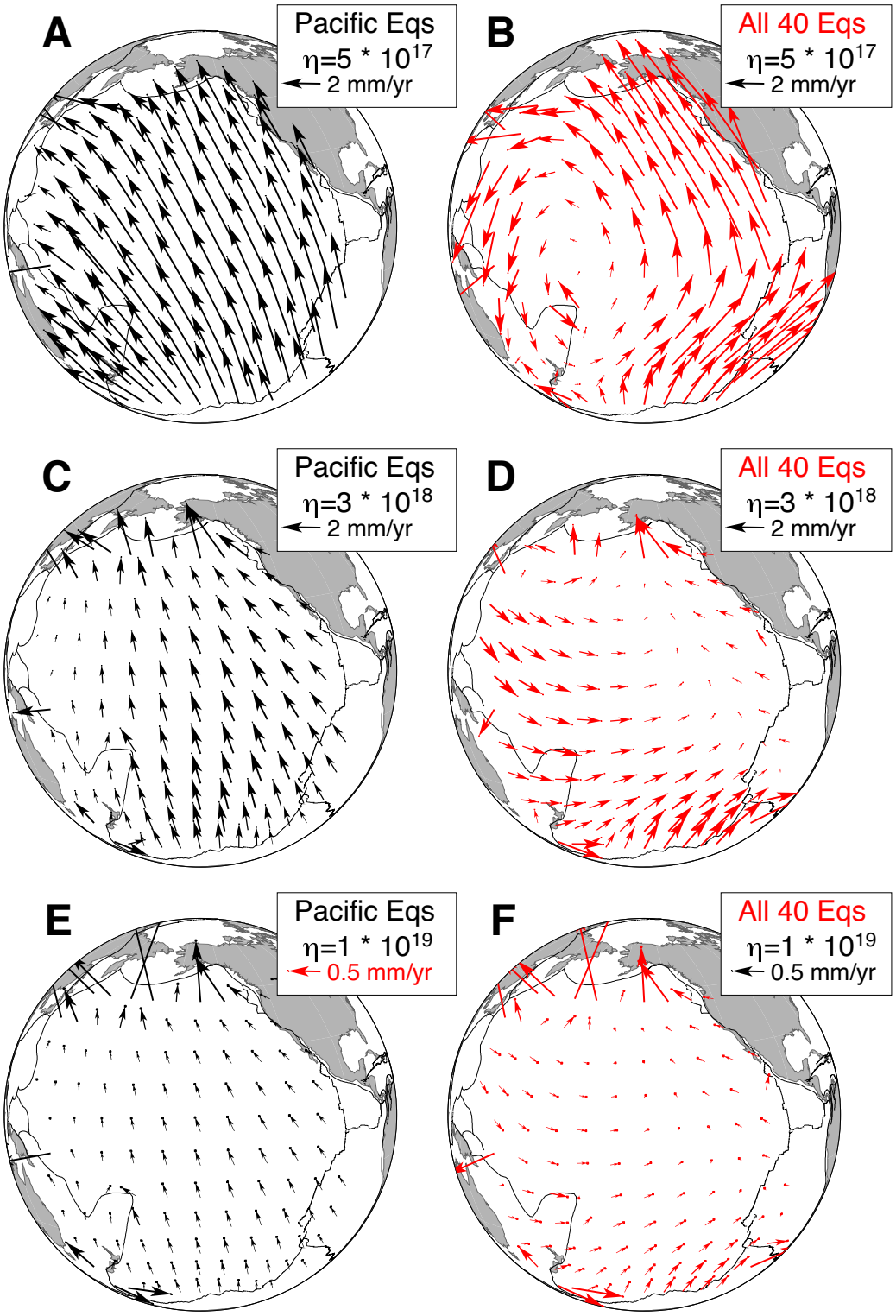

Figure 11. Average velocities from 1994 to 2014 of the horizontal viscoelastic surface deformation for three assumed asthenospheric viscosities η and two possible earthquake groupings, consisting of either all the earthquakes listed in Table 3 and shown in in Fig. 9 or only those earthquakes from the boundaries of the Pacific Plate (red squares in Fig. 9). The velocity at a given grid node is determined by summing the daily viscoelastic motion predicted at the node for each earthquake during the period 1994 January 1 and 2014 January 1. Differences between the patterns for the six models are discussed in Section 4.6.3.

4.7 Testing for tectonic deformation within the Pacific Plate

Finally, we considered alternative geometries for the Pacific Plate that include a deforming zone that subdivides the plate into two smaller, non-deforming plates. We defined seven alternative two-plate geometries that are based on plausible groupings of the 28 GPS sites on the Pacific Plate and compared the relative fits of these geometries from inversions of the GPS velocities. These included

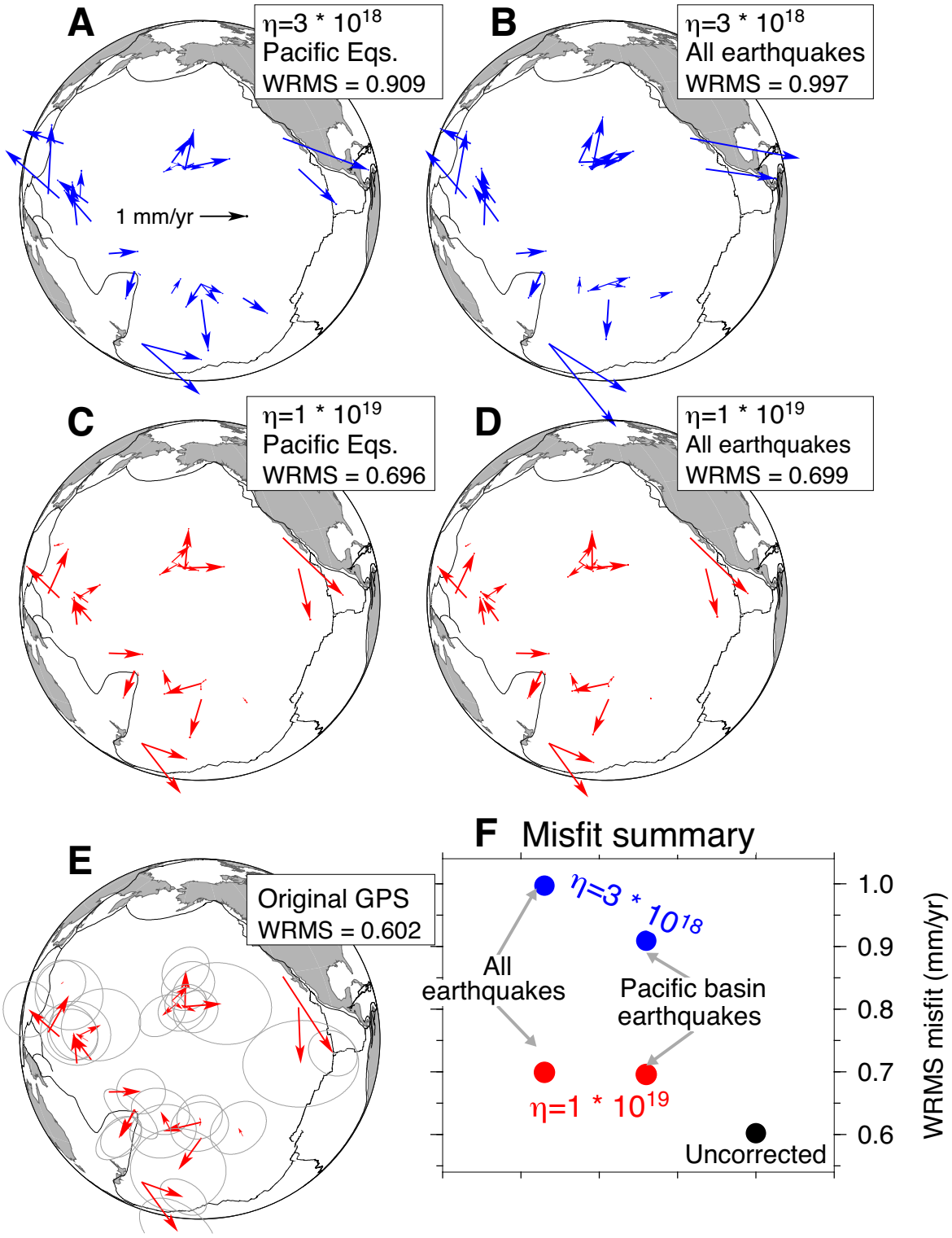

Figure 12. GPS site velocities relative to the Pacific Plate (a–e) and WRMS misfit summary (f). Globes (a) and (b) show residual GPS site velocities after correcting the Pacific Plate GPS velocity field for viscoelastic deformation calculated for an assumed asthenospheric viscosity of 3×10^{18} Pa s. Globes (c) and (d) similarly show residual velocities for an assumed asthenospheric viscosity of 1×10^{19}. In (a) and (c), corrections are made only for the 25 Pacific basin earthquakes indicated by the red symbols in Fig. 9. In (b) and (d), corrections are made for all 40 earthquakes in Table 3 and Fig. 9. Globe (e) shows the GPS velocities relative to the Pacific Plate interior absent any correction for viscoelastic deformation (also see Fig. 6). Panel (f) summarizes the WRMS misfits for the residual velocities shown in Globes (a) to (e). The WRMS misfits for corrections that are based on an assumed asthenospheric viscosity of 5×10^{17} Pa s are not shown, but are 2.8 and 1.5 mm yr^{-1} for the two earthquake groupings (Section 4.6.4), much worse than for the other five models.

one geometry already described and tested above (Section 4.2), in which the velocities for Clarion and Guadalupe islands in the eastern Pacific basin are fit separately from the velocities of the 26 sites elsewhere on the Pacific Plate.

Of the seven two-plate geometries that we tested, only one passes the *F*-ratio test for an additional plate at the 99 per cent confidence level, namely, the geometry that isolates Clarion and Guadalupe islands from the remaining 26 Pacific Plate sites. Distributing $\sim$1 mm yr^{-1} of deformation across the 4000–9000 km distances between Clarion/Guadalupe islands and the remaining Pacific Plate sites would require an intraplate strain rate of only $\sim 2 \times 10^{-10}$ strain yr^{-1}.

5 DISCUSSION

Our new GPS velocity field imposes useful new limits on strain rates within the Pacific Plate. The 26 Pacific Plate sites whose velocities are used to estimate the Pacific Plate angular velocity (Section 4.1) span a maximum distance of 9000 km in any direction and are all located on seafloor older than 30 Myr. Their WRMS velocity misfit of 0.6 mm yr^{-1} implies an approximate 1σ limit of 7×10^{-11} yr^{-1} for strain rates within the areas of the Pacific Plate that are older than $\approx$30 Myr. The low strain rate agrees well with estimates for other plates (Gordon 1998) and is consistent with the low rate of seismicity within the Pacific Plate during the past century (Wysession *et al.* 1991).

The motions of Clarion and Guadalupe Islands, which move with an average weighted velocity of 1.7 ± 0.5 mm yr^{-1} towards S17°E $\pm$ 11° relative to the plate interior, give an upper (95 per cent) limit of $\approx 2 \times 10^{-10}$ yr^{-1} for intraplate strain along a great circle that spans the Pacific Plate from east to west (Fig. 1). Their southward motions towards older seafloor in the southern and central Pacific suggest that intraplate strain is predominantly contractional and south-to-north. Any east–west contractional (or extensional) component across the Pacific is below the resolution of our velocity field.

Horizontal thermal contraction that accompanies cooling of oceanic plates may explain the southward motions of Clarion and Guadalupe islands (Kumar & Gordon 2009). Widely accepted as the cause of age-dependent seafloor subsidence (e.g. Parsons & Sclater 1977; Stein & Stein 1992), conductive cooling of oceanic plates may also cause measurable, isotropic horizontal seafloor contraction given a large-enough expanse of young seafloor such as exists in the eastern Pacific basin (Kumar & Gordon 2009). In particular, an integration of age-dependent, thermal contractional strain rates along a 9000-km-long great circle that follows a $\sim$5-Myr-old seafloor isochron west of the East Pacific and Pacific–Antarctica rises suggests that young seafloor in the eastern Pacific basin adjacent to North America could move several millimetres per year to the south relative to older seafloor in the southern Pacific (Kumar & Gordon 2009).

The southward movements of Clarion and Guadalupe Islands (e.g. Fig. 2) are qualitatively consistent with ridge-parallel contraction of young seafloor along the East Pacific Rise and Pacific–Antarctic rise, as predicted by Kumar & Gordon (2009). A more rigourous determination of the expected rate and direction of thermal contraction at 12.5-Myr-old Guadalupe Island and 13.5-Myr-old Clarion Island will require modeling of the 2-D pattern of thermal contraction for the whole Pacific Plate based on its dimensions, geometry and seafloor age distribution. Such a calculation is beyond the scope of this paper.

6 CONCLUSIONS

Our synthesis of new and existing observations from Clarion, Guadalupe and Socorro islands, the only three locations on the Pacific Plate where GPS observations sample the motion of seafloor younger than 20 Myr, yields several useful new results. Weekly positions from 1993 to late 2009 of a DORIS beacon located only 0.75 km from our GPS site on Socorro Island indicate that the site motion is dominated by transient volcanic deformation associated with a 1993–1996 eruption of the island's shield volcano (Fig. 4). By implication, our Socorro Island GPS site velocity is unsuitable for tectonic studies. In contrast, measurements that span 15.6 yr at Clarion Island and 12.0 yr at Guadalupe Island, which are separated by 1225 km, give remarkably similar velocities (Figs 2 and 3) that differ at high confidence level from the motions expected if they moved with the Pacific Plate. With respect to plate motion that is defined from the velocities of 26 stations that are well distributed in the central, southern, and western Pacific, the average weighted velocity for Clarion and Guadalupe islands is 1.7 ± 0.5 mm yr^{-1} towards S17°E $\pm$ 11°.

Tests of alternative hypotheses for the apparent motions of both islands, including possible drift of Earth's origin in ITRF08, the influence of fault locking along the Pacific-North America Plate boundary, possible biases in our GPS site velocities due to unmodelled, small offsets from large earthquakes since 2000, and viscoelastic deformation from 40 $M \geq 8$ earthquakes in and near the Pacific basin since 1950, all fail to explain the southward motions of Clarion and Guadalupe islands relative to the Pacific Plate interior and in some cases degrade the fit of a best-fitting angular velocity to the new Pacific Plate velocity field. Our viscoelastic modelling strongly excludes viscosities lower than 1×10^{19} Pa s for the asthenosphere below the Pacific Plate over time scales of several years or longer; stated differently, we find no evidence for long-wavelength viscoelastic perturbations in the present-day Pacific Plate GPS velocity field from large historic earthquakes at an approximate threshold of 0.3–0.5 mm yr^{-1}.

The southward motions of Clarion and Guadalupe islands are qualitatively consistent with the expectation that horizontal thermal contraction of the Pacific Plate should include a contractional component parallel to the East Pacific and Pacific–Antarctic rises, such that young seafloor adjacent to western North America should move southward towards older seafloor in the southern Pacific (Kumar & Gordon 2009). Our results call for a more rigourous test of this hypothesis. Alternatively, the motions of Clarion and Guadalupe islands may be caused by slow, distributed intraplate deformation due to tectonic forces. Misfits within areas of the Pacific Plate that are spanned by the 26 GPS sites whose velocities define its motion suggest an approximate 95 per cent upper bound on the intraplate strain rate of 1×10^{-10} yr^{-1}, comparable to that estimated for other plate interiors.

ACKNOWLEDGEMENTS

This work originated as an effort to quantify seismic hazard in western California from the perspective of the Pacific Plate. It was funded partly by Pacific Gas and Electric. Support for this project was also provided by UNAM's PAPIT project IN104213-2 and NSF grant EAR-1114174. We are grateful to the following agencies and individuals for their assistance in occupying the GPS stations on Clarion and Socorro Islands: CONANP, Biol. Maria Jossue Navarro Sanchez, Reserva de la Biosfera Archipielago de Revillagigedo; Secretaria de Gobernacion, Direccion de

Coordinacion Politica con los Poderes de la Union; SEMAR, Jefe del Estado Mayor General, Luis Salazar Tlaczani, Felipe Arriaga, Martin Baltazar, Francisco Correa-Mora, Guillermo Fong, Francisco Nunez and Susana Perez. We also thank Centro de Estudios Estrategicos para el Desarrollo CEED of Universidad de Guadalajara for logistical and financial support. We thank Paul Tregoning and Saskia Goes for their constructive reviews. We thank Fred Pollitz for open access to his Visco1D code and useful tips on using the code, the International DORIS service (http://ids-doris.org) for making their weekly DORIS solutions available (Willis *et al.* 2010), and Rocco Malservisi for assistance in linking the GUAX and GAIR GPS time-series. Figures were drafted using Generic Mapping Tools software (Wessel & Smith 1991). We are grateful for open access to continuous GPS data from a variety of sources, including the following: (1) the Plate Boundary Observatory operated by UNAVCO and supported by National Science Foundation grants EAR-0350028 and EAR-0732947, (2) the Global GNSS Network operated by UNAVCO for NASA Jet Propulsion Laboratory under NSF Cooperative Agreement No. EAR-0735156, (3) SONEL (www.sonel.org), (4) The GeoNet project of New Zealand (www.geonet.org.nz), (5) Centre National d'Etudes Spatiales of France, (5) Geospatial Information Authority, Japan and (6) Universite de Polynesis Francaise.

REFERENCES

Abe, K., 1973. Tsunami and mechanism of great earthquakes, *Phys. Earth planet. Int.,* **7,** 143–153.

Altamimi, Z., Sillard, P. & Boucher, C., 2002. ITRF2000: a new release of the International Terrestrial Reference Frame for Earth science applications, *J. geophys. Res.,* **107,** 2214, doi:10.1029/2001JB000561.

Altamimi, Z., Collilieux, X. & Metivier, L., 2011. ITRF2008: An improved solution of the International Terrestrial Reference Frame, *J. Geod.,* **8,** 457–473.

Argus, D.F., 1996. Postglacial uplift and subsidence of Earth's surface using VLBI geodesy: on establishing vertical reference, *Geophys. Res. Lett.,* **23,** 973–976.

Argus, D.F. & Gordon, R.G., 1996. Tests of the rigid-plate hypothesis and bounds on intraplate deformation using geodetic data from Very Long Baseline Interferometry, *J. geophys. Res.,* **101,** 13 555–13 572.

Argus, D.F. *et al.*, 1999. Shortening and thickening of metropolitan Los Angeles measured by using geodesy, *Geology,* **27,** 703–706.

Argus, D.F., Gordon, R.G., Heflin, M.B., Ma, C., Eanes, R., Willis, P., Peltier, W.R. & Owen, S.E., 2010. The angular velocities of the plates and the velocity of Earth's centre from space geodesy, *Geophys. J. Int.,* **180**(3), 913–960.

Banerjee, P., Pollitz, F., Nagarajan, B. & Burgmann, R., 2007. Coseismic slip distributions of the 26 December 2004 Sumatra-Andaman and 28 March 2005 Nias earthquakes from GPS static offsets, *Bull. seism. Soc. Am.,* **97,** S86–S102.

Beavan, J., Tregoning, P., Bevis, M., Kato, T. & Meertens, C., 2002. Motion and rigidity of the Pacific plate and implications for plate boundary deformation, *J. geophys. Res.,* **107**(B10), doi:10.1029/2001JB000282.

Beavan, J., Wang, X., Holden, C., Wilson, K., Power, W., Prasetya, G., Bevis, M. & Kautoke, R., 2010. Near-simultaneous great earthquakes at Tongan megathrust and outer rise in September 2009, *Nature,* **466,** 959–963. *Geochem. Geophys. Geosys.,* **10,** Q09007, doi:10.1029/2009GC002373.

Beck, S.L. & Christensen, D.H., 1991. Rupture process of the February 4, 1965, Rat Islands earthquake, *J. geophys. Res.,* **96,** 2205–2221.

Beck, S.L. & Ruff, L.J., 1984. The rupture process of the great 1979 Colombia earthquake: evidence for the asperity model, *J. geophys. Res.,* **89,** 9281–9291.

Beck, S.L. & Ruff, L.J., 1989. Great earthquakes and subduction along the Peru trench, *Phys. Earth planet. Int.,* **57,** 199–224.

Briole, P., Willis, P., Dubois, J. & Charade, O., 2009. Potential volcanological applications of the DORIS system: a geodetic study of the Socorro Island, Mexico) coordinate time series, *Geophys. J. Int.,* **178,** 581–590.

Buck, W.R., Small, C. & Ryan, W.B.F., 2009. Constraints on asthenospheric flow from the depths of oceanic spreading centers: the East Pacific Rise and the Australian-Antarctic Discordance, *Geochem. Geophys. Geosyst.*, **10**, Q09007, doi:10.1029/2009GC002373.

DeMets, C. & Dixon, T., 1999. New kinematic models for Pacific-North America motion from 3 Ma to present, 1: evidence for steady motion and biases in the NUVEL-1A model, *Geophys. Res. Lett.,* **26,** 1921–1924.

DeMets, C., Gordon, R.G. & Argus, D.F., 2010. Geologically current plate motions, *Geophys. J. Int.,* **181,** 1–80.

DeMets, C., Marquez-Azua, B. & Cabral-Cano, E., 2014. A new GPS velocity field for the Pacific Plate – Part 2: implications for fault slip rates in western California, *Geophys. J. Int.,* doi:10.1093/gji/ggu347.

Dixon, T., Farina, F., DeMets, C., Suarez Vidal, F., Fletcher, J., Marquez-Azua, B., Miller, M., Sanchez, O. & Umhoefer, P., 2000. New kinematic models for Pacific-North America motion from 3 Ma to present, II: tectonic implications for Baja and Alta California, *Geophys. Res. Lett.,* **27,** 3961–3964.

Dziewonski, A.M. & Anderson, D.L., 1981. Preliminary reference earth model, *Phys. Earth planet. Int.,* **25,** 297–356.

Freed, A.M. & Burgmann, R., 2004. Evidence of power-law flow in the Mojave desert mantle, *Nature,* **430,** 548–551.

Freed, A.M., Burgmann, R., Calais, E., Freymueller, J. & Hreinsdottir, S., 2006. Implications of deformation following the 2002 Denali, Alaska, earthquake for postseismic relaxation process and lithospheric rheology, *J. geophys. Res.,* **111,** B01401, doi:10.1029/2005JB003894.

Freed, A.M., Herring, T. & Burgmann, R., 2010. Steady-state laboratory flow laws alone fail to explain postseismic observations, *Earth planet. Sci. Lett.,* **300,** 1–10.

Fujii, Y. & Satake, K., 2013. Slip distribution and seismic moment of the 2010 and 1960 Chilean earthquakes inferred from tsunami waveforms and coastal geodetic data, *Pure appl. Geophys.,* **170,** 1493–1509.

Fukao, Y. & Furumoto, M., 1979. Stress drops, wave spectra, and recurrence intervals of great earthquakes—implications of the Etorofu earthquake of 1958 November 6, *Geophys. J. R. astr. Soc.,* **57,** 23–40.

Furlong, K.P., Lay, T. & Ammon, C.J., 2009. A great earthquake rupture across a rapidly evolving three-plate boundary, *Science,* **324,** 226–229.

Gaherty, J.B., Jordan, T.H. & Gee, L.S., 1996. Seismic structure of the upper mantle in a central Pacific corridor, *J. geophys. Res.,* **101,** 22 291–22 309.

Geist, E.L. & Parsons, T., 2005. Triggering of tsunamigenic aftershocks from large strike-slip earthquakes: analysis of the November 2000 New Ireland earthquake sequence, *Geochem. Geophys. Geosys.,* **6,** Q10005, doi:10.1029/2005GC000935.

Gonzalez-Garcia, J.J., Prawirodirdjo, L., Bock, Y. & Agnew, D., 2003. Guadalupe Island, Mexico, as a new constraint for Pacific plate motion, *Geophys. Res. Lett.,* **30,** doi:10.1029/2003GL017732.

Gordon, R.G., 1998. The plate tectonic approximation: plate nonrigidity, diffuse plate boundaries, and global plate reconstructions, *Annu. Rev. Earth Planet. Sci.,* **26,** 615–642.

Heki, K., 1996. Horizontal and vertical crustal movements from three-dimensional very long baseline interferometry kinematic reference frame: implication for the reversal time scale revision, *J. geophys. Res.,* **101,** 3187–3198.

Henry, C. & Das, S., 2002. The M_w 8.2, 17 February 1996 Biak, Indonesia, earthquake: rupture history, aftershocks, and fault plane properties, *J. geophys. Res.,* **107,** doi:10.1029/2001JB000796.

Hirth, G. & Kohlstedt, D.L., 1996. Water in the oceanic upper mantle: Implications for rheology, melt extraction, and the evolution of the lithosphere, *Earth planet. Sci. Lett.,* **144,** 93–108.

Hutton, W., DeMets, C., Sanchez, O., Suarez, G. & Stock, J., 2001. Slip kinematics and dynamics during and after the 1995 October 9 $M_w = 8.0$ Colima-Jalisco earthquake, Mexico, from GPS geodetic constraints, *Geophys. J. Int.,* **146,** 637–658.

Hwang, L.J. & Kanamori, H., 1986. Of the May 7, 1986 Andreanof Islands earthquake source parameters, *Geophys. Res. Lett.,* **13,** 1426–1429.

Johnson, J.M. & Satake, K., 1993. Source parameters of the 1957 Aleutian earthquake from tsunami waveforms, *Geophys. Res. Lett.,* **20,** 1487–1490.

Kanamori, H., 1970. Synthesis of long-period surface waves and its application to earthquake source studies—Kurile Islands earthquake of October 13, 1963, *J. geophys. Res.,* **75,** 5011–5027.

Kanamori, H., 1971. Focal mechanism of the Tokachi-Oki earthquake of May 16, 1968: contortion of the lithosphere at a junction of two trenches, *Tectonophys.,* **12,** 1–13.

Kanamori, H., 1976. Re-examination of the Earth's free oscillations excited by the Kamchatka earthquake of November 4, 1952, *Phys. Earth planet. Int.,* **11,** 216–226.

Kikuchi, M. & Kanamori, H., 1995. The Shikotan earthquake of October 4, 1994: lithospheric earthquake, *Geophys. Res. Lett.,* **22,** 1025–1028.

Klitgord, K. & Mammerickx, J., 1982. Northern East Pacific Rise: magnetic anomaly and bathymetric framework, *J. geophys. Res.,* **87,** 6725–6750.

Koketsu, K., Hikima, K., Miyazaki, S. & Ide, S., 2004. Joint inversion of strong motion and geodetic data for the source process of the 2003 Tokachi-oki, Hokkaido, earthquake, *Earth Planets Space,* **56,** 329–334.

Konca, A.O. *et al.*, 2008. Partial rupture of a locked patch of the Sumatra megathrust during the 2007 earthquake sequence, *Nature,* **456,** 631–635.

Kumar, R.V. & Gordon, R.G., 2009. Horizontal thermal contraction of oceanic lithosphere: the ultimate limit to the rigid plate approximation, *J. geophys. Res.,* **114,** B01403, doi:10.1029/2007JB005473.

Kyriakopoulos, C., Masterlark, T., Stramondo, S., Chini, M. & Bignami, C., 2013. Coseismic slip distribution for the M_w 9 2011 Tohoku-Oki earthquake derived from 3-D FE modeling, *J. geophys. Res. Solid Earth,* **118,** 3837–3847.

Larson, K. M., Freymueller, J.T. & Philipsen, S., 1997. Global plate velocities from the Global Positioning System, *J. geophys. Res.,* **102,** 9962–9982.

Lay, T., Kanamori, H., Ammon, C.J., Hutko, A.R., Furlong, K. & Rivera, L., 2009. The 2006–2007 Kuril Islands great earthquake sequence, *J. geophys. Res.,* **114,** B11308, doi:10.1029/2008JB006280.

Lay, T., Ammon, C.J., Kanamori, H., Rivera, L., Koper, K.D. & Hutko, A.R., 2010. The 2009 Samoa-Tonga great earthquake triggered doublet, *Nature,* **466,** 964–968.

Lonsdale, P., 1991. Structural patterns of the Pacific floor offshore of Peninsular California, in *Gulf and Peninsula Provinces of the Californias*, AAPG Memoir 47, pp. 87–125. eds Dauphin, J.P. & Simoneit, B.R.T., AAPG.

Lorito, S. *et al.*, 2011. Limited overlap between the seismic gap and coseismic slip of the great 2010 Chile earthquake, *Nat. Geosci.,* **4,** 173–177.

Mammerickx, J., Naar, J.F. & Tyce, R.L., 1988. The Mathematician paleoplate, *J. geophys. Res.,* **93,** 3025–3040.

Mao, A., Harrison, C.G.A. & Dixon, T.H., 1999. Noise in GPS coordinate time series, *J. geophys. Res.,* **104,** 2797–2816.

Marquez-Azua, B., Cabral-Cano, E., Correa-Mora, F. & DeMets, C., 2004. A model for Mexican neotectonics based on nationwide GPS measurements, 1993-2001, *Geof. Int.,* **43,** 319–330.

Mendoza, C., Hartzell, S. & Monfret, T., 1994. Wide-band analysis of the 3 March 1985 central Chile earthquake: overall source process and rupture history, *Bull. seism. Soc. Am.,* **84,** 269–283.

Mendoza, C. & Hartzell, S.H., 1989. Slip distribution of the 19 September 1985 Michoacan, Mexico, earthquake: near-source and teleseismic constraints, *Bull. seism. Soc. Am.,* **79,** 655–669.

Miyazaki, S., McGuire, J.J. & Segall, P., 2011. Seismic and aseismic fault slip before and during the 2011 off the Pacific coast of Tohoku earthquake, *Earth Planets Space*, **63,** 637–642.

Muller, R.D., Roest, W.R., Royer, J.-Y., Gahagan, L.M. & Sclater, J.G., 1997. Digital isochrons of the world's ocean floor, *J. geophys. Res.,* **102,** 3211–3214.

Parsons, B. & Sclater, J.G., 1977. An analysis of the variation of ocean floor bathymetry and heat flow with age, *J. geophys. Res.,* **82,** 803–827.

Plattner, C., Malservisi, R., Dixon, T.H., LaFemina, P., Sella, G., Fletcher, J. & Vidal-Suarez, F., 2007. New constraints on relative motion between the Pacific plate and Baja California microplate, Mexico) from GPS measurements, *Geophys. J. Int.,* **170,** 1373–1380.

Pollitz, F.F., 1997. Gravitational viscoelastic postseismic relaxation on a layered spherical Earth, *J. geophys. Res.,* **102,** 17 921–17 941.

Pollitz, F.F., Burgmann, R. & Romanowicz, B., 1998. Viscosity of oceanic asthenosphere inferred from remote triggering of earthquakes, *Science,* **280,** 1245–1249.

Pollitz, F.F., Burgmann, R. & Banerjee, P., 2006. Post-seismic relaxation following the great 2004 Sumatra-Andaman earthquake on a compressible self-gravitating Earth, *Geophys. J. Int.,* **167,** 397–420.

Pritchard, M.E., Simons, M., Rosen, P.A., Hensley, S. & Webb, F.H., 2002. Co-seismic slip from the 1995 July 30 $M_w = 8.1$ Antofagasta, Chile, earthquake as constrained by InSAR and GPS observations, *Geophys. J. Int.,* **150,** 362–376.

Pritchard, M.E., Norabuena, E.O., Ji, C., Boroschek, R., Comte, D., Simons, M., Dixon, T.H. & Rosen, P.A., 2007. Geodetic, teleseismic, and strong motion constraints on slip from recent southern Peru subduction zone earthquakes, *J. geophys. Res.,* **112,** B03307, doi: 10.1029/2006JB004294.

Ryan, J.W., Clark, T.A., Ma, C., Gordon, D., Caprette, D.S. & Himwich, W.E., 1993. Global scale tectonic plate motions measured with CDP VLBI data, in *Contributions of Space Geodesy to Geodynamics: Crustal Dynamics (Geodynamics Series),* eds. Smith, D.E. & Turcotte, D.L., American Geophysical Union, Washington, doi:10.1029/GD023p0037.

Schwartz, S.Y., Dewey, J.W. & Lay, T., 1989. Influence of fault plane heterogeneity on the seismic behavior in the southern Kurile islands arc, *J. geophys. Res.,* **94,** 5637–5649.

Shimazaki, K., 1974. Pre-seismic crustal deformation caused by an underthrusting oceanic plate in eastern Hokkaido, Japan, *Phys. Earth planet. Int.,* **8,** 148–157.

Sladen, A. *et al.*, 2010. Source model of the 2007 M_w 8.0 Pisco, Peru, earthquake: implications for seismogenic behavior of subduction megathrusts, *J. geophys. Res.,* **115,** B02405, doi:10.1029/2009JB006429.

Smith, D. E. *et al.*, 1990. Tectonic motion and deformation from satellite laser ranging to LAGEOS, *J. geophys. Res.,* **95,** 22 013–22 041.

Stein, S. & Gordon, R.G., 1984. Statistical tests of additional plate boundaries from plate motion inversions, *Earth planet. Sci. Lett.,* **69,** 401–412.

Stein, C.A. & Stein, S., 1992. A model for the global variation in oceanic depth and heat flow with lithospheric ages, *Nature,* **359,** 123–129.

Tan, Y. & Helmberger, D.V., 2007. Trans-Pacific upper mantle shear velocity structure, *J. geophys. Res.,* **112,** B08301, doi:10.1029/2006JB004853.

Tang, L. *et al.*, 2008. Tsunami forecast analysis for the May 2006 Tonga tsunami, *J. geophys. Res.,* **113,** C12015, doi:10.1029/2008JC004922.

Tregoning, P., 2002. Plate kinematics in the western Pacific derived from GPS observations, *J. geophys. Res.,* **107,** doi:10.1029/JB2001000406.

Tregoning, P., Burgette, R., McClusky, S.C., Lejeune, S., Watson, C.S. & McQueen, H., 2013. A decade of horizontal deformation from great earthquakes, *J. geophys. Res. Solid Earth,* **118,** 2371–2381.

Velasco, A.A., Ammon, C.J. & Lay, T., 1995. Source time function complexity of the great 1989 Macquarie Ridge earthquake, *J. geophys. Res.,* **100,** 3989–4009.

Wang, L., Shum, C.K., Simons, F.J., Tapley, B. & Dai, C., 2012. Coseismic and postseismic deformation of the 2011 Tohoku-Oki earthquake constrained by GRACE gravimetry, *Geophys. Res. Lett.,* **39,** L07301, doi:10.1029/2012GL051104.

Ward, S.N., 1990. Pacific-North America plate motions: new results from very long baseline interferometry, *J. geophys. Res.,* **95,** 21 965–21 981.

Wessel, P. & Smith, W.H.F., 1991. Free software helps map and display data, *EOS, Trans. Am. geophys. Un.,* **72,** 441–446.

Willis, P. *et al.*, 2010. The International DORIS Service, Toward maturity, in DORIS: Scientific Applications in Geodesy and Geodynamics, ed. Willis, P., *Adv. Space Res.,* **45,** 1408–1420.

Wu, X., Collilieux, X., Altamimi, Z., Vermeersen, B. L. A., Gross, R.S. & Fukumori, I., 2011. Accuracy of the International Terrestrial Reference Frame origin and Earth expansion, *Geophys. Res. Lett.,* **38,** L13304, doi:10.1029/2011GL047450.

Wysession, M.E., Okal, E.A. & Miller, K.L., 1991. Intraplate seismicity of the Pacific basin, *Pure appl. Geophys.,* **135,** 261–359.

Zumberge, J.F., Heflin, M.B., Jefferson, D.C., Watkins, M.M. & Webb, F.H., 1997. Precise point positioning for the efficient and robust analysis of GPS data from large networks, *J. geophys. Res.,* **102,** 5005–5017.

SUPPORTING INFORMATION

Additional Supporting Information may be found in the online version of this article:

ggu341Earthquake_Info.pdf
ggu341PacGPS_Supplement_Fiile1.pdf

(http://gji.oxfordjournals.org/lookup/suppl/doi:10.1093/gji/ggu341/-/DC1).

Please note: Oxford University Press is not responsible for the content or functionality of any supporting materials supplied by the authors. Any queries (other than missing material) should be directed to the corresponding author for the article.